Tumor-associated macrophages drive spheroid formation during early transcoelomic metastasis of ovarian cancer

Mingzhu Yin,[1] Xia Li,[1] Shu Tan,[1,2] Huanjiao Jenny Zhou,[1,3,4] Weidong Ji,[3,4] Stefania Bellone,[5] Xiaocao Xu,[1] Haifeng Zhang,[1] Alessandro D. Santin,[5] Ge Lou,[2] and Wang Min[1,3,4]

[1]Department of Pathology and Vascular Biology and Therapeutics Program, Yale University School of Medicine, New Haven, Connecticut, USA. [2]Department of Gynecology Oncology, The Tumor Affiliated Hospital of Harbin Medical University, Harbin, China. [3]Center for Translational Medicine, The First Affiliated Hospital, Sun Yat-sen University, Guangzhou, China. [4]Guangzhou Darron Medscience Co., Guangzhou, China. [5]Department of Obstetrics, Gynecology, and Reproductive Sciences, Yale Cancer Center, Yale University School of Medicine, New Haven, Connecticut, USA.

Tumor-associated macrophages (TAMs) can influence ovarian cancer growth, migration, and metastasis, but the detailed mechanisms underlying ovarian cancer metastasis remain unclear. Here, we have shown a strong correlation between TAM-associated spheroids and the clinical pathology of ovarian cancer. Further, we have determined that TAMs promote spheroid formation and tumor growth at early stages of transcoelomic metastasis in an established mouse model for epithelial ovarian cancer. M2 macrophage–like TAMs were localized in the center of spheroids and secreted EGF, which upregulated $\alpha_M\beta_2$ integrin on TAMs and ICAM-1 on tumor cells to promote association between tumor cells and TAM. Moreover, EGF secreted by TAMs activated EGFR on tumor cells, which in turn upregulated VEGF/VEGFR signaling in surrounding tumor cells to support tumor cell proliferation and migration. Pharmacological blockade of EGFR or antibody neutralization of ICAM-1 in TAMs blunted spheroid formation and ovarian cancer progression in mouse models. These findings suggest that EGF secreted from TAMs plays a critical role in promoting early transcoelomic metastasis of ovarian cancer. As transcoelomic metastasis is also associated with many other cancers, such as pancreatic and colon cancers, our findings uncover a mechanism for TAM-mediated spheroid formation and provide a potential target for the treatment of ovarian cancer and other transcoelomic metastatic cancers.

Introduction

Ovarian cancer (OC) is the second most common gynecological cancer and the leading cause of death in the United States (1, 2). Its high mortality rate is mainly due to the difficulty of diagnosis of OC at early stages (I/II) until it spreads and advances to later stages (III/IV) (3). We also reported that the diagnosis rates for patients with OC from stage I to IV are 7.19%, 8.63%, 72%, and 12.18%, respectively (4, 5). The prognosis for OC is poor. The 5-year survival rate for all stages of OC is 42% (6). Long-term follow-up of suboptimally debulked stage III and stage IV patients showed a 5-year survival rate of less than 10% (7). However, for patients diagnosed at early stages (I–II), particularly when the cancer is still confined to the primary site, the 5-year survival rate is 92.7% (3). Studies revealed that the 5-year survival rate of OC has increased less than 2% as compared with that in last decade. The major reason for the poor prognosis of OC is intraperitoneal and extensive pelvic implantation metastasis, which is usually unable to be removed completely by surgery. In such cases, tumor cytoreductive surgery is the last option for most OC patients. So far, there are no effective drugs specifically targeting implantation metastasis, while the current drugs for chemotherapy of OC easily induce drug resistance and have poor prognosis long term. Therefore, it is essential to elucidate the mechanism of OC transcoelomic metastasis, which is also critical for developing novel drugs for targeting OC transcoelomic metastasis and improving the survival rate for OC.

The most widely ascribed explanation for the phenomenon of peritoneal metastasis is that tumor cells become detached from the primary tumor after extension into the peritoneal surface and are transported throughout the peritoneal cavity by peritoneal fluid before seeding i.p. Many studies have suggested that the process of transcoelomic metastasis could be divided into several steps: (a) cell detachment, survival, and resistance of anoikis; (b) evasion of immunological surveillance; (c) epithelial-mesenchymal transition; (d) spheroid formation; (e) ascites formation; and (f) peritoneal implantation (8–10). However, it remains unclear how free detached tumor cells survive in the transcoelomic environment and form spheroids in the initial steps of transcoelomic metastasis. Our objective is to define the mechanism of OC transcoelomic metastasis using mouse orthotopic OC models. Our present study reveals that macrophages play an essential role in the survival and proliferation of free cells detached from the primary tumor in the transcoelomic environment and in spheroid formation at early stages of transcoelomic metastasis.

Results

Macrophages are involved in spheroid formation during OC growth. To determine whether macrophages participate in OC survival, proliferation, and implantation during transcelomic

Authorship note: M. Yin, X. Li, and S. Tan contributed equally to this work.
Conflict of interest: The authors have declared that no conflict of interest exists.
Submitted: February 24, 2016; **Accepted:** August 30, 2016.
Reference information: *J Clin Invest*. 2016;126(11):4157–4173. doi:10.1172/JCI87252.

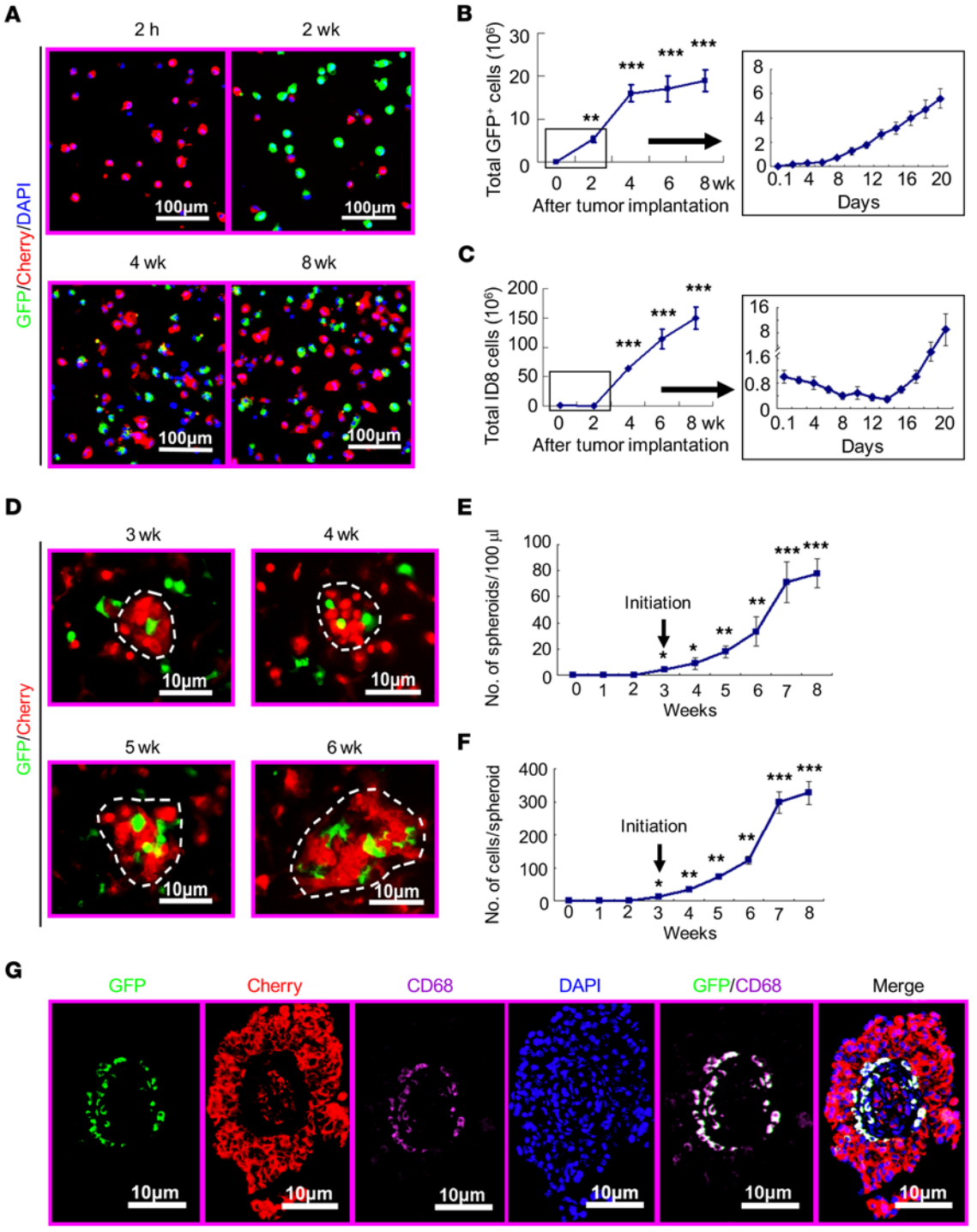

Figure 1. Macrophages are involved in spheroid formation in an orthotopic OC model. ID8 OCs stably expressing mCherry fluorescence protein were implanted into 8-week-old tomato$^{LysM\text{-}Cre}$ recipient mice. Cherry$^+$ tumor cells and GFP$^+$ cells infiltrated into the peritoneal cavity were detected at 2, 4, 6, and 8 weeks after tumor cell implantation. (**A**) Peritoneal cells were smeared on slides and were observed under a fluorescence microscope. Representative images are shown. n = 5 mice for each time point. (**B**) The total number of GFP$^+$ cells was quantified. Inset shows cell counting from days 0–20. n = 5 mice for each time point. (**C**) The total number of Cherry$^+$ tumor cells was quantified. Inset shows cell counting from days 0–20. n = 5 mice for each time point. (**D**–**G**) Macrophage and spheroid formation. Representative fluorescence images from weeks 3 to 6 are shown in **D**. Total number of spheroids (spheroids/100 μl ascites) (**E**) and size of spheroids (number of cells/spheroid) (**F**) were quantified. n = 5 mice for each time point. Initiation of spheroid formation at week 3 is indicated. (**G**) Spheroids collected at week 8 were subjected to immunostaining with APC-conjugated (647 nm) anti-CD68 and DAPI, followed by confocal imaging. GFP$^+$ and CD68$^+$ macrophages, Cherry$^+$ tumor cells, and DAPI for nuclear staining are shown. A merged image is shown on the right. All data are presented as mean ± SEM. n = 5. *P < 0.05; **P < 0.01; ***P < 0.001 (2-sided Student's t test).

metastasis, we established an orthotopic mouse model in which mouse ID8 OC cells were i.p. injected into C57BL/6 female recipient mice. To trace cancer cells and recipient monocytes/macrophages during these stages, ID8 OC cells were labeled by stably expressing mCherry fluorescence protein while *LysM-Cre* mice crossed to the tomato reporter *mT/mG* (referred to as tomato$^{LysM\text{-}Cre}$ mice) were used as recipients in which myeloid cells, including macrophages, were labeled with GFP (11). GFP$^+$ cells in the peritoneal cavities of tomato$^{LysM\text{-}Cre}$ recipient mice were barely detectable at the basal state (prior to tumor cell injection) or at early times (<1 week) after tumor injection. However, GFP$^+$ cells infiltrated into the peritoneal cavity were drastically increased at 2, 4, 6 and 8 weeks after tumor injection, and the total numbers of GFP$^+$ cells were 3×10^6, 16×10^6, 18×10^6, 20×10^6 at 2, 4, 6 and 8 weeks, respectively (Figure 1, A and B). Since *LysM-Cre* is a myeloid-specific deleter, we confirmed that the majority (~80%) of GFP$^+$ cells infiltrated into the peritoneal cavity were F4/80$^+$, CD11b$^+$, and CD68$^+$ macrophages at 2 to 8 weeks, as detected by FACS (Supplemental Figure 1, A and B for 8 weeks; supplemental material available online with this article; doi:10.1172/JCI87252DS1). We also detected increased CD11b$^+$Gr1$^+$ myeloid-derived suppressor cells (MDSCs) (12, 13) in ascites at advanced stages (6 week) (Supplemental Figure 1, C and D). In this orthotopic OC model, injected cancer cells exhibited an initial quiescent stage (at 0–2 weeks) followed by a rapid growing phase (at 2–8 weeks after tumor injection) (Figure 1C), mimicking human stages II–III of OC (3). Interestingly, we observed an initial decline in the number of tumor cells in the peritoneal cavity between 2 hours and 2 weeks after tumor injection, likely due to anoikis (8). The total number of tumor cells started to increase at 3 weeks after implantation when tumor clusters (spheroids) were detected in the ascites (Supplemental Figure 2). Microscopic examination indicated that spheroids contained both GFP$^+$ macrophages and mCherry tumor cells with a ratio of approximately 1:10; the number and size of spheroids were increased during tumor growth (Figure 1D with quantifications in Figure 1, E and F). Intriguingly, immunostaining of the spheroid sections indicated that mCherry tumor cells within the large spheroids surrounded the center-located GFP$^+$CD68$^+$ macrophages (Figure 1G). Similar results were obtained for CD11b$^+$Gr1$^+$ MDSCs. These results suggest that the interactions between myeloid cells and ID8 cells promote spheroid formation during the process of OC transcoelomic seeding.

Accumulation of M2 subtype TAMs correlates with OC progression. We detected macrophages in the peritoneal cavity at 2 hours after tumor injection of tumor cells, yet macrophages seemed to promote tumor cell growth only after 3 weeks after tumor injection, when the macrophage-tumor spheroids were formed. Previous reports suggest that OC cells polarize macrophages toward an M2 phenotype in vitro and in vivo (14, 15). We reasoned that macrophages in the spheroid formation phase had gene expression profiles and phenotypes that were distinct from those of the initial phase. To this end, we harvested F4/80$^+$CD11b$^+$ macrophages at various phases of OC growth (1, 4, and 8 weeks after tumor injection), and a set of M1 subtype–specific and M2 subtype–specific markers was examined by quantitative reverse-transcriptase PCR (qRT-PCR). Peripheral blood monocytes were used as a control. Results indicated that the initial infiltrated macrophages (at 1 week) induced by tumor cells strongly expressed M1-like marker genes (*Ly6g/c*, *Ccr2*, *Ifnar*, *iNOS*), but these markers were lost after 4 weeks. However, infiltrated macrophages gradually gained expression of M2-like marker genes (*Cd206* [mannose receptor], *Cx3cr1*, arginase 1, and *Cd163* [scavenger receptor cysteine-rich type 1 protein M130]) during tumor progression (4–8 weeks). Of note, both individual and spheroid-associated macrophages at late stages (8 weeks) had similar gene expression profiles (Figure 2A). FACS analysis and immunostaining confirmed distinct expression patterns for early CCR2$^+$ and late CD163$^+$, CD206$^+$, and CX3CR1$^+$ tumor–induced macrophages (Figure 2, B and C, and Supplemental Figure 3, A and B). These results suggest that tumor-associated macrophages (TAMs) were polarized to the M2-like subtype in the peritoneal cavity microenvironment during OC progression.

TAMs are essential for peritoneal spheroid formation and tumor growth of OC. To explore the role of TAMs in the process of OC transcoelomic metastasis, tumor-bearing mice were treated with liposome clodronate (LC), as was done previously (16). LC had no direct inhibitory effects on tumor cells in vitro (Supplemental Figure 4, A and B). Complete blood cell counting and FACS analyses indicated that LC specifically and effectively depleted monocytes/macrophages, but not T cells, from circulation and the peritoneal cavity in mice (Supplemental Figure 5, A and B). Phenotype analyses showed that LC significantly reduced mouse total body weight, ascitic fluid volume, and wet weight of tumor cells isolated from the ascitic fluid (Figure 3, A–C). Accordingly, mouse survival rate was greatly increased by clodronate treatment (Figure 3D). Notably, the number and average size of spheroids were significantly smaller in the clodronate group compared with the liposome group (Figure 3, E–G). Further studies revealed that Ki67$^+$ cells were tumor cells that surrounded CD68$^+$ TAMs in the spheroid, and both CD68$^+$ TAMs and Ki67$^+$ cells were diminished by clodronate treatment (Figure 3, H–J).

We then directly tested to determine whether TAMs promote spheroid formation and OC progression. To this end, F4/80$^+$CD206$^+$ M2 TAMs (15) (1×10^6) isolated from the spheroids of OC-bearing donor mice were coinjected with ID8 cells (1×10^6) into the peritoneal cavities of new recipient mice. Recipient mice were treated with liposome or treated with LC (Supplemental Figure 6). Injections of TAMs or ID8 cells were used as controls. Injection of TAMs alone did not produce tumors (not shown), suggesting that the isolated TAMs were pure without contaminated ID8 cells. The TAMs+ID8 group markedly augmented tumor growth, accumulation of ascitic fluid, and net tumor weight compared with the ID8 group. However, the LC-treated group had lower body weights, ascitic fluid volume, and tumor weights than the TAM$^+$ ID8 group and even the ID8 group (Figure 3, A–C). These data suggest that LC diminished effects of both exogenous and endogenous TAMs on OC growth. TAMs also shortened the survival of tumor-bearing mice, but this effect was prolonged by LC (Figure 3D). Moreover, the number and size of tumor spheroids and CD68$^+$ macrophage and Ki67$^+$ tumor cells inside the spheroids were significantly increased by TAMs, but were diminished by clodronate (Figure 3, E–G). TAMs also enhanced Ki67$^+$ tumor cells that attached to or surrounded CD68$^+$ macrophages in

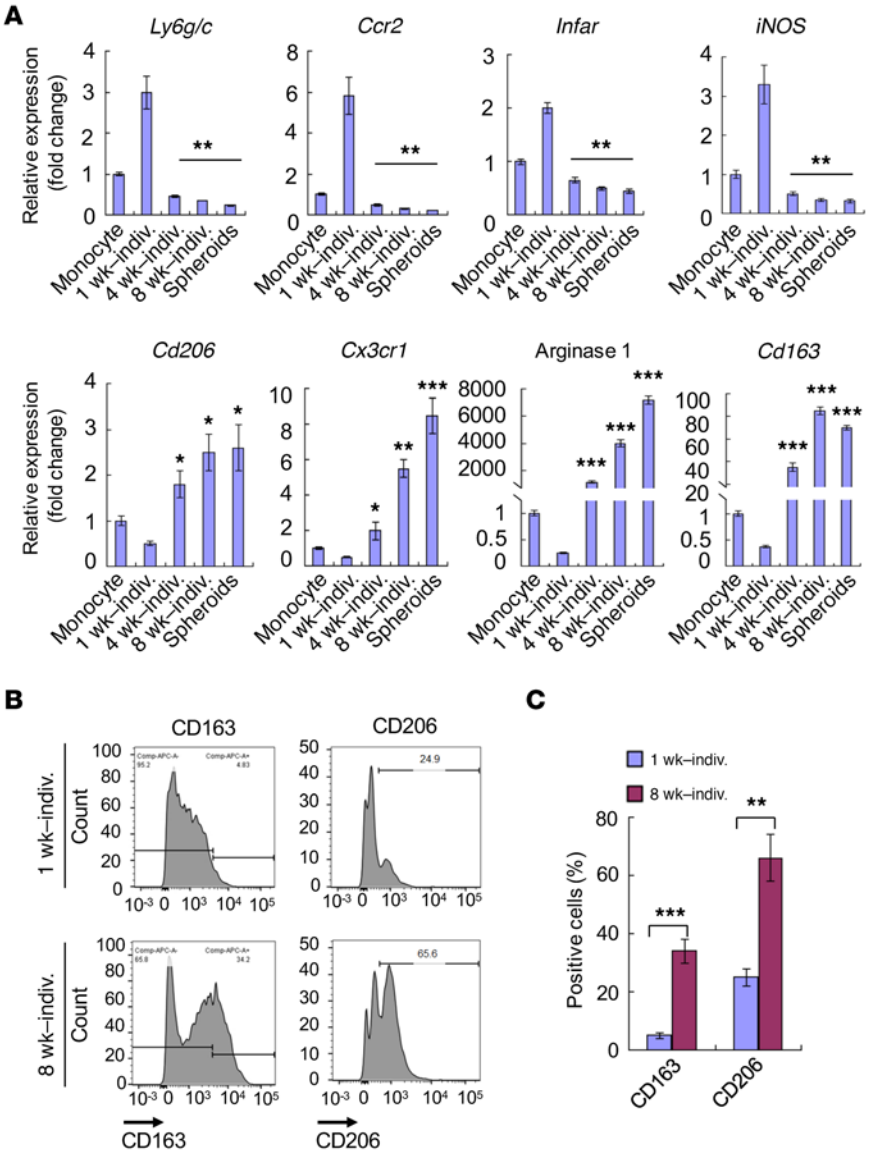

Figure 2. Accumulation of M2 subtype TAMs correlates with OC progression. F4/80$^+$ CD11b$^+$ macrophages in the orthotopic OC model were harvested from individual cell populations or spheroids at the indicated times (1, 4, and 8 weeks). (**A**) M1 subtype–specific and M2 subtype–specific markers were determined by qRT-PCR. Peripheral blood monocytes were used as a control. All data are presented as mean ± SEM. $n = 5$. $^*P < 0.05$; $^{**}P < 0.01$; $^{***}P < 0.001$ (2-sided Student's t test) comparing with gene expression in week 1 individual (indiv) cells. (**B** and **C**) FACS and statistical analysis of CD163 and CD206 expression in macrophages from week 1 and 8 individual cells. All data are presented as mean ± SEM. $n = 5$. $^*P < 0.05$; $^{**}P < 0.01$; $^{***}P < 0.001$ (2-sided Student's t test).

the spheroid. However, both Ki67$^+$ cells and CD68$^+$ macrophages were diminished by clodronate treatment (Figure 3, H–J). Taken together, these data suggest that macrophages are essential for OCs in peritoneal spheroid formation and cell proliferation.

Reciprocal upregulation of EGF in TAMs and EGFR in tumor cells is critical for tumor growth. To define the molecular mechanism by which TAMs promote OC proliferation, we determined effects of F4/80$^+$CD206$^+$M2 TAMs on ID8 cells isolated from the spheroids in peritoneal cavity (PE-ID8) in a Transwell assay where macrophages and tumor cells were not directly contacted. ID8 OC cells that had been cultured in vitro (naive ID8) were used as a control. Although F4/80$^+$CD206$^+$ TAMs had a weak effect on naive ID8, F4/80$^+$CD206$^+$ TAMs significantly promoted PE-ID8 cell growth as determined by total cell number (Figure 4A). F4/80$^+$CD206$^+$ TAMs increased tumor cell proliferation as measured by Ki67 immunostaining staining (Figure 4, B and C).

We reasoned that TAMs in the spheroids provide growth factors to support spheroid formation and tumor cell proliferation. We therefore screened the expression pattern of various growth factors in TAMs and ID8 ovarian tumor cells isolated from the peritoneal cavity (PE-ID8) by qRT-PCR. We found that only *Egf*, but not other growth factors, such as *Fgfs*, *Hgf*, *Igf*, *Tnfa*, *Tgfb*, or *Vegfs*, were detected in TAMs (Supplemental Figure 7A). *Egf* was highly expressed in spheroid-derived F4/80$^+$CD206$^+$ TAMs, but not in spheroid-derived PE-ID8 as detected by qRT-PCR. Reciprocally, *Egfr* was highly expressed in spheroid-derived PE-ID8 cells, but not in TAMs (Figure 4D). Immunostaining of spheroids confirmed that EGF was specifically detected in TAMs that were surrounded by EGFR$^+$ tumor cells (Figure 4E). We detected secreted EGF in ascitic fluid at a much higher concentration than plasma EGF as detected by ELISA (Supplemental Figure 7B). Consistent with the results from qRT-PCR, EGF was not detected in culture supernatant of spheroid-derived PE-ID8. EGF was detected from the supernatant of F4/80$^+$CD206$^+$ TAMs and was further enhanced by coculture with ID8 tumor cells (Supplemental Figure 7C). We next tested to determine whether F4/80$^+$CD206$^+$ TAMs promote PE-ID8 tumor cell proliferation through the EGF/EGFR axis. To this end, EGF expression

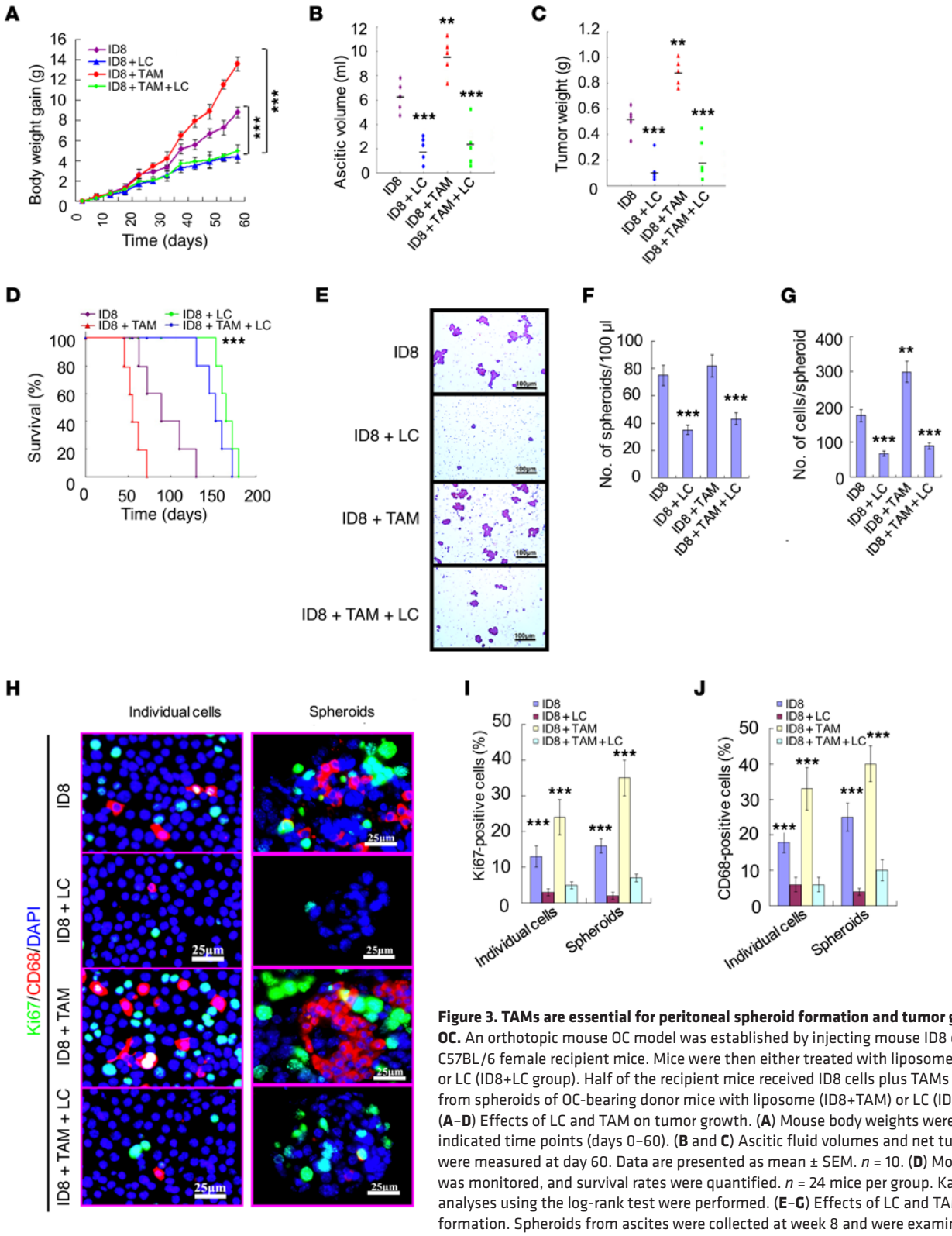

Figure 3. TAMs are essential for peritoneal spheroid formation and tumor growth of OC. An orthotopic mouse OC model was established by injecting mouse ID8 cells i.p. into C57BL/6 female recipient mice. Mice were then either treated with liposome (ID8 group) or LC (ID8+LC group). Half of the recipient mice received ID8 cells plus TAMs isolated from spheroids of OC-bearing donor mice with liposome (ID8+TAM) or LC (ID8+TAM+LC). (**A**–**D**) Effects of LC and TAM on tumor growth. (**A**) Mouse body weights were measured at indicated time points (days 0–60). (**B** and **C**) Ascitic fluid volumes and net tumor weights were measured at day 60. Data are presented as mean ± SEM. $n = 10$. (**D**) Mouse modality was monitored, and survival rates were quantified. $n = 24$ mice per group. Kaplan-Meier analyses using the log-rank test were performed. (**E**–**G**) Effects of LC and TAM on spheroid formation. Spheroids from ascites were collected at week 8 and were examined by H&E staining (**E**). Total number (**F**) and size (**G**) of spheroids were quantified. Scale bars: 100 μm. (**H**–**J**) Effects of LC and TAM on tumor cell proliferation. Individual cells and spheroids collected at week 8 were subjected to immunostaining with anti-Ki67, anti-CD68, and DAPI, followed by confocal imaging. (**H**) Representative images showing $CD68^+$ macrophages are surrounded by $Ki67^+$ tumor cells in ID8 but not in ID8+LC group. Scale bars: 25 μm. $Ki67^+$ (**I**) and $CD68^+$ cells (**J**) in individual and spheroid populations were quantified. $n = 5$ mice and 10 spheroids from each mice. Data are presented as mean ± SEM. $^{**}P < 0.01$; $^{***}P < 0.001$ (2-sided Student's t test).

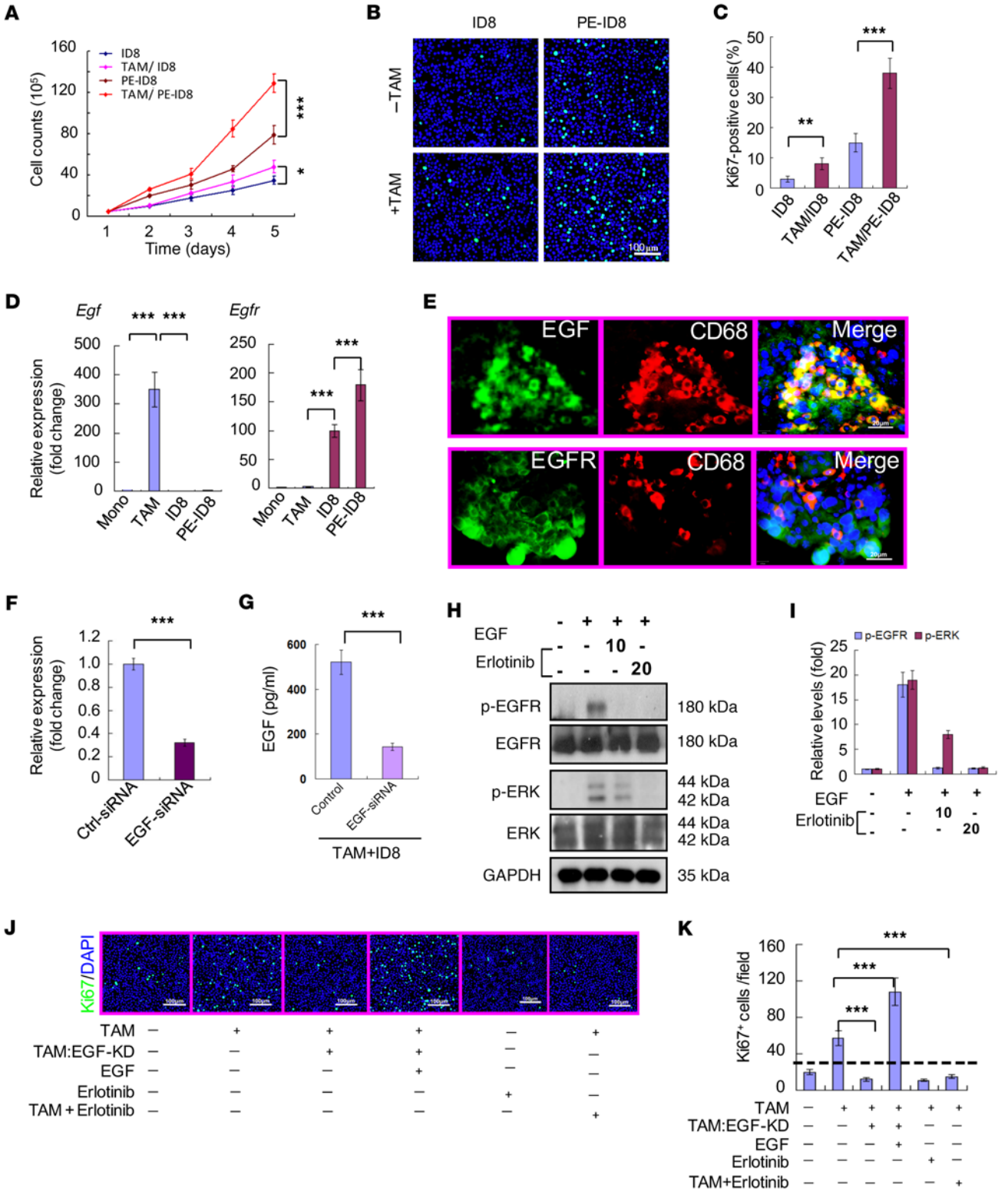
A
Cell counts (10^5)
ID8
TAM/ ID8
PE-ID8
TAM/ PE-ID8
Time (days)
B
ID8
PE-ID8
−TAM
+TAM
C
Ki67-positive cells (%)
ID8
TAM/ID8
PE-ID8
TAM/PE-ID8
D
Egf
Egfr
Relative expression (fold change)
Mono
TAM
ID8
PE-ID8
E
EGF
CD68
Merge
EGFR
F
Relative expression (fold change)
Ctrl-siRNA
EGF-siRNA
G
EGF (pg/ml)
Control
EGF-siRNA
TAM+ID8
H
EGF
Erlotinib
p-EGFR
EGFR
p-ERK
ERK
GAPDH
180 kDa
44 kDa
42 kDa
35 kDa
I
p-EGFR
p-ERK
Relative levels (fold)
J
Ki67/DAPI
TAM
TAM:EGF-KD
EGF
Erlotinib
TAM + Erlotinib
K
Ki67+ cells /field
TAM
TAM:EGF-KD
EGF
Erlotinib
TAM+Erlotinib

Figure 4. Reciprocal upregulation of *Egf* in TAMs and *Egfr* expression in tumor cells are critical for OC growth. (**A**–**C**) TAMs promote ID8 cell proliferation in vitro. Peritoneal spheroids were harvested from OC-bearing mice at 8 weeks after tumor implantation. TAMs and ID8 tumor cells (PE-ID8) were isolated, and PE-ID8 cells were cultured alone or cocultured with TAMs in a Transwell without direct contacts. Naive ID8 cells were used as controls. (**A**) Total cell number was counted at times indicated. (**B**) Cell proliferation was measured by Ki67 staining. Scale bar: 100 μm. (**C**) Ki67$^+$ tumor cells were quantified. n = 9. (**D**) Reciprocal upregulation of EGF in TAMs and EGFR expression in PE-ID8 cells. Gene expression of *Egf* and *Egfr* in TAMs and PE-ID8 was determined by qRT-PCR. Peripheral blood monocytes and naive ID8 tumor cells were used as controls. Relative gene expression is presented as fold change in relation to monocytes as 1.0. n = 3. (**E**) Immunofluorescent staining of CD68 with EGF or EGFR in spheroids harvested from ascites of OC mice. Representative images of spheroids from n = 5 mice are shown. Scale bar: 20 μm. (**F** and **G**) KD of EGF by siRNAs. TAMs were transfected with control (ctrl) or EGF siRNAs for 48 hours. (**F**) *Egf* mRNA levels in TAMs detected by qRT-PCR. (**G**) EGF protein levels in supernatant of TAMs cocultured with ID8 cells were measured by ELISA. (**H** and **I**) ID8 cells were treated with EGF in the absence or presence of EGFR inhibitor (10 or 20 μM) for 12 hours. Phospho- and total EGFR and ERK1/2 were determined by Western blot with respective antibodies. Total EGFR, ERK1/2, and GAPDH were determined. Relative phosphorylation levels were quantified. (**J** and **K**) TAMs were pretransfected with control siRNA or EGF siRNA. PE-ID8 cells were cultured alone or cocultured with TAMs in a Transwell in the absence or presence of EGF (20 ng/ml) or EGFR inhibitor (20 μM) for 12 hours. Proliferating PE-ID8 cells were stained by Ki67. Representative images are shown (**J**) with quantification of Ki67$^+$ cells (**K**). Scale bars: 100 μm. Three different replicates were performed for all experiments. Data are presented as mean ± SEM. $^*P < 0.05$; $^{**}P < 0.01$; $^{***}P < 0.001$ (2-sided Student's t test).

in TAMs was knocked down (KD) with siRNAs, whereas EGFR signaling in PE-ID8 cells was blocked by the EGFR inhibitor erlotinib. EGF silencing in TAMs by 2 sets of siRNAs was verified by qRT-PCR and ELISA (Figure 4, F and G). The effect of erlotinib on EGF/EGFR signaling in ID8 cells was verified by phosphorylation of EGFR and ERK1/2 (Figure 4, H and I). Importantly, TAM-stimulated proliferation of PE-ID8 tumor cells was completely blunted by either the knocking down of EGF in TAMs or the treatment of ID8 with erlotinib (Figure 4, J and K).

Clinical relevance of spheroid formation between EGF$^+$ TAMs and EGFR$^+$ tumor cells in OC patients. To investigate our observation that spheroid formation between EGF$^+$ TAMs and EGFR$^+$ tumor cells exists in human OC patients, we examined spheroids isolated from ascites of 128 OC patients. Immunohistochemical (IHC) staining of CD68 showed that macrophages were present in nearly all spheroids we collected. Moreover, the macrophage number was significantly higher in spheroids than in the primary tumor (Figure 5, A and B). Similarly to the mouse model, most CD68$^+$ macrophages were gathered in the center of spheroids (Figure 5C), supporting that macrophages play an important role in initiating spheroid formation during the transcoelmic metastasis of OC. By staining with CD68 and Ki67 in different sizes (small, medium, and large) of spheroids isolated from ascites, the markers for macrophage and proliferating cells, a clear positive correlation between TAMs and proliferating tumor cells was observed (Figure 5, C and D). To investigate the possible correlation between TAM-associated spheroid and clinical pathology of OC, we analyzed percentages of TAMs in spheroids isolated from 128 OC patients with good, moderate, or poor histological differentiation. The demographic and clinical characteristics of patients are listed in Supplemental Table 1. The number of CD68$^+$ cells increased with lymphovascular invasion (LVI) (P = 0.013), ascite volume (P = 0.009), and serum levels of cancer antigen 125 (CA-125, an early marker for OC in women with a very high risk of the disease) (P = 0.0043) in spheroids from OC patients. Quantification of CD68-positive cells in spheroids from OC patients with good, moderate, and poor histological differentiation revealed that the percentage of CD68$^+$ cells in spheroids was greater in poorly differentiated OC compared with more-differentiated OCs (Figure 5, E and F), suggesting that poorly differentiated OC might attract more macrophages in spheroid formation compared with well-differentiated OC. However, there was no observed difference in TAM counts according to histology type (P = 0.134) and chemotherapy regimen (P = 0.21) (Supplemental Table 1). Further, uni- and multivariate analysis revealed that the 5-year overall survival (OS) rate was significantly lower in OC patients with high percentages (>14.5%) as compared with low percentages (< 14.5%) of CD68-positive cells in spheroids (Figure 5G and Supplemental Table 2 and Supplemental Table 3).

Inhibition of EGFR reduces spheroid formation and ovarian tumor growth in mouse models. Given the association of spheroid formation between EGF$^+$ TAMs and EGFR$^+$ tumor cells in both mouse models and human OC patients, we tested to determine whether the EGFR inhibitor could block spheroid formation and tumor growth. Erlotinib (EGFR inhibitor) inhibited proliferation of most OC cell lines, whereas gefitinib and cetuximab inhibited the proliferation of a part of OC cell lines (17, 18). We chose erlotinib to define the role of EGFR in the process of OC transcoelomic metastasis. To this end, we first tested effects of erlotinib on tumor OC progression in the aforementioned ID8 model and a xenograft mouse model in which SKOV3 human OCs were i.p. injected into a female recipient nude model. Erlotinib was coinjected with tumor cells into the peritoneal cavities of recipient mice (Supplemental Figure 8). Similar to the syngeneic mouse models, human OC growth was substantially retarded when TAMs were depleted with LC. Furthermore, the inhibitory effect of LC on tumor growth was more effective when LC was given at an early stage (2 weeks after tumor implantation) compared with administration of LC at late times (4–8 weeks) (Figure 6A). Similarly to LC, the EGFR inhibitor erlotinib drastically retarded the ovarian tumor growth with higher efficiencies when it was administrated at earlier time points (Figure 6B). Ascitic fluid volume and tumor weight were significantly reduced with increased survival in erlotinib-treated mice as compared with untreated groups in both models (Figure 6, C–E and Supplemental Figure 9, A–D). We further analyzed spheroid formation, cancer cell proliferation, and OC progression with erlotinib treatments. Both the number and size of spheroids were significantly reduced by erlotinib in the mouse models (Figure 6, F–H, and Supplemental Figure 9, E–G). Total numbers of TAMs and Ki67$^+$ proliferative cancer cells either individually or in the spheroids were drastically reduced by erlotinib (Figure 6, I–J, and Supplemental Figure 9, H–J). These results suggest that TAM-secreted EGF plays a critical role for spheroid formation, cancer cell proliferation, and tumor growth at an early stage of transcoelomic metastasis of OC.

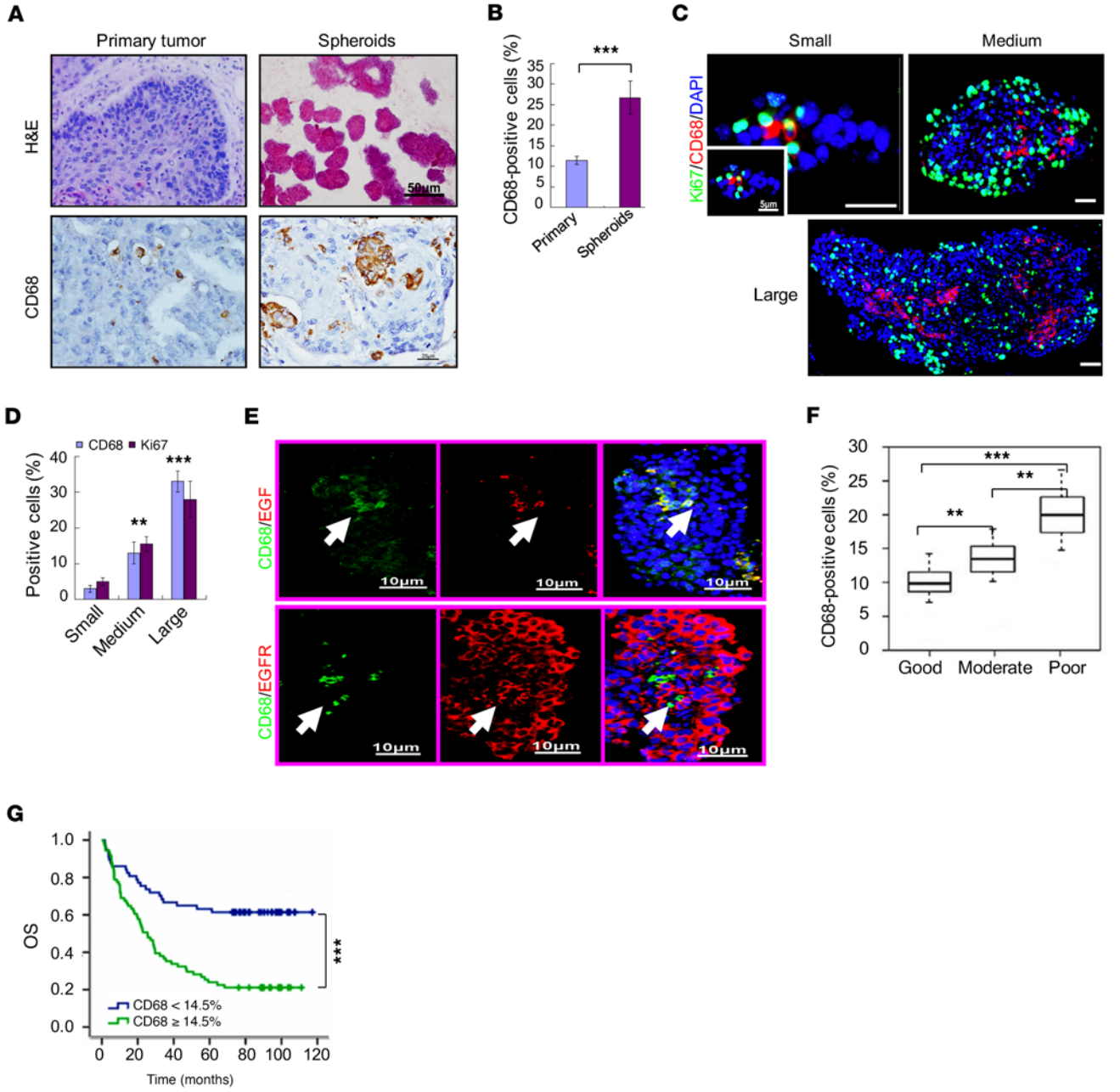

Figure 5. Clinical relevance of spheroid formation between EGF$^+$ TAMs and EGFR$^+$ tumor cells in OC patients. (**A** and **B**) Macrophages and spheroids in human OC. (**A**) H&E and CD68 IHC staining of primary tumors and spheroids isolated from OC patients. Scale bars: 50 μm (H&E); 25 μm (CD68). (**B**) Statistical analysis of CD68-positive cells in primary tumors and spheroids of OC patients. $n = 128$. Data are presented as mean ± SEM. $^{***}P < 0.001$ (2-sided Student's t test). (**C** and **D**) Correlations between macrophages and cancer cell proliferation in spheroids. (**C**) Immunostainings of CD68 and Ki67 in small, medium, and large spheroids of human OC. DAPI is used for nucleus staining. Representative images are shown. Scale bars: 5 μm. (**D**) Quantifications of CD68- and Ki67-positive cells in spheroids. $n = 30$. Small spheroid (0–50 cells/spheroid); medium cell cluster (50–500 cells/spheroid); large spheroid (≥500 cells/spheroid). Data are presented as mean ± SEM. $^{**}P < 0.01$; $^{***}P < 0.001$ (2-sided Student's t test) comparing medium and large spheroids with small spheroids. (**E**) Immunofluorescent staining of spheroids harvested from ascites of OC patients. Costainings of CD68 with EGF or EGFR (**E**). Representative images of spheroids from $n = 128$ OC patients are shown. CD68$^+$EGF$^+$ TAMs in the center of spheroids are indicated by arrows. Scale bars: 10 μm. (**F**) Statistical analysis of CD68$^+$ cells in OC spheroids with different histological differentiation (2-sided Student's t test, **A**–**F**). (**G**) Kaplan-Meier curves for OS in 128 OC patients with low (≤14.5%) or high (≥14.5%) percentage of CD68$^+$ cells in OC spheroids (analyzed with log-rank test)

EGF promotes EGFR$^+$ tumor cell migration and TAM spheroid formation through VEGF-C/VEGFR3 signaling. We next examined how TAM-produced EGF mediates spheroid formation, which is essential for initial OC growth. Our data indicate that TAMs were located at the center of clusters and that the number and size of spheroids were markedly reduced by the EGFR inhibitor erlotinib in OC models. Based on these observations, we hypothesized that TAM-secreted EGF mediates tumor cell migration toward TAMs and adhesion to TAMs, a prerequisite step involved in spheroid formation. To define the molecular mechanism by

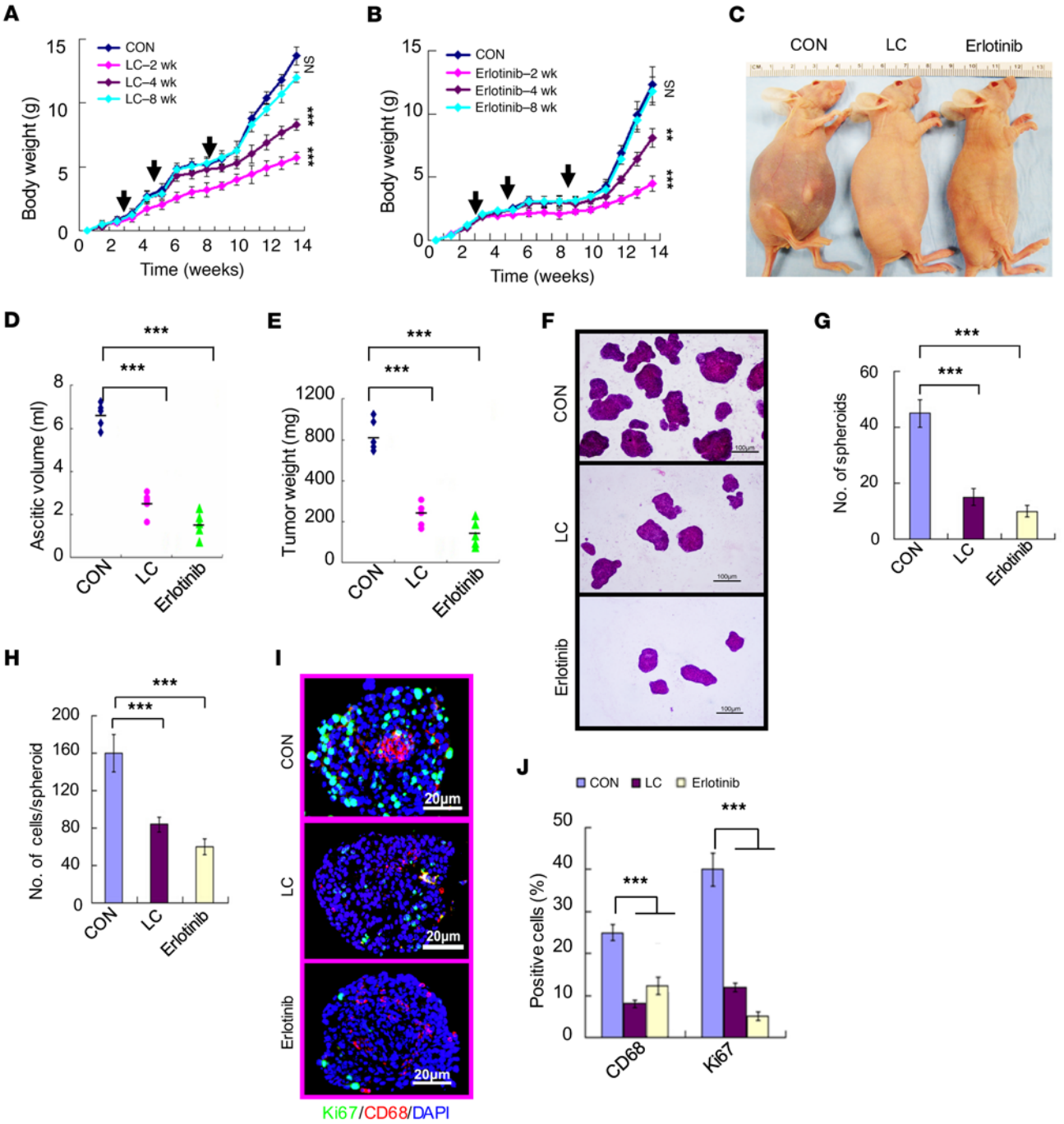

Figure 6. Inhibition of EGFR reduces spheroid formation, cell proliferation, and ovarian tumor growth in mouse models. An orthotopic mouse model was established by injecting human SKOV3 OCs i.p. into female recipient nude mice. Mice were then either untreated (CON) or treated with erlotinib i.p. (100 mg/kg body weight/d). LC was used as a treatment control. (**A**–**E**) Effects of erlotinib on SKOV3 tumor growth. (**A** and **B**) Mouse body weights were measured at indicated time points. Arrows indicate different starting times of treatment (2, 4, or 8 weeks after tumor cell implantation) with LC (**A**) or erlotinib (**B**). (**C**) Representative images of mouse bodies in control, LC-, and erlotinib-treated groups. (**D** and **E**) Ascitic fluid volumes and net tumor weights were measured at week 14. Data in **A**–**E** are presented as mean ± SEM. $n = 10$ for each group. $^{***}P < 0.001$. (**F**–**H**) Effects of erlotinib on SKOV3 spheroid formation. Spheroids from ascites were collected at week 14 and mounted on slides. Spheroids were examined by H&E staining (**F**). Scale bars: 100 μm. Total number (**G**) and size (**H**) of spheroids were quantified. (**I** and **J**) Effects of erlotinib on SKOV3 tumor cell proliferation. Spheroids collected at week 14 were subjected to immunostaining with anti-Ki67, anti-CD68, and DAPI, followed by confocal imaging. (**I**) Representative images of spheroids with Ki67$^+$ tumor cells and CD68$^+$ macrophages. (**J**) Ki67$^+$ and CD68$^+$ cells in spheroids were quantified. $n = 5$ mice and 10 spheroids from each mice. Data are presented as mean ± SEM. $^{**}P < 0.01$;$^{***}P < 0.001$ (2-sided Student's t test).

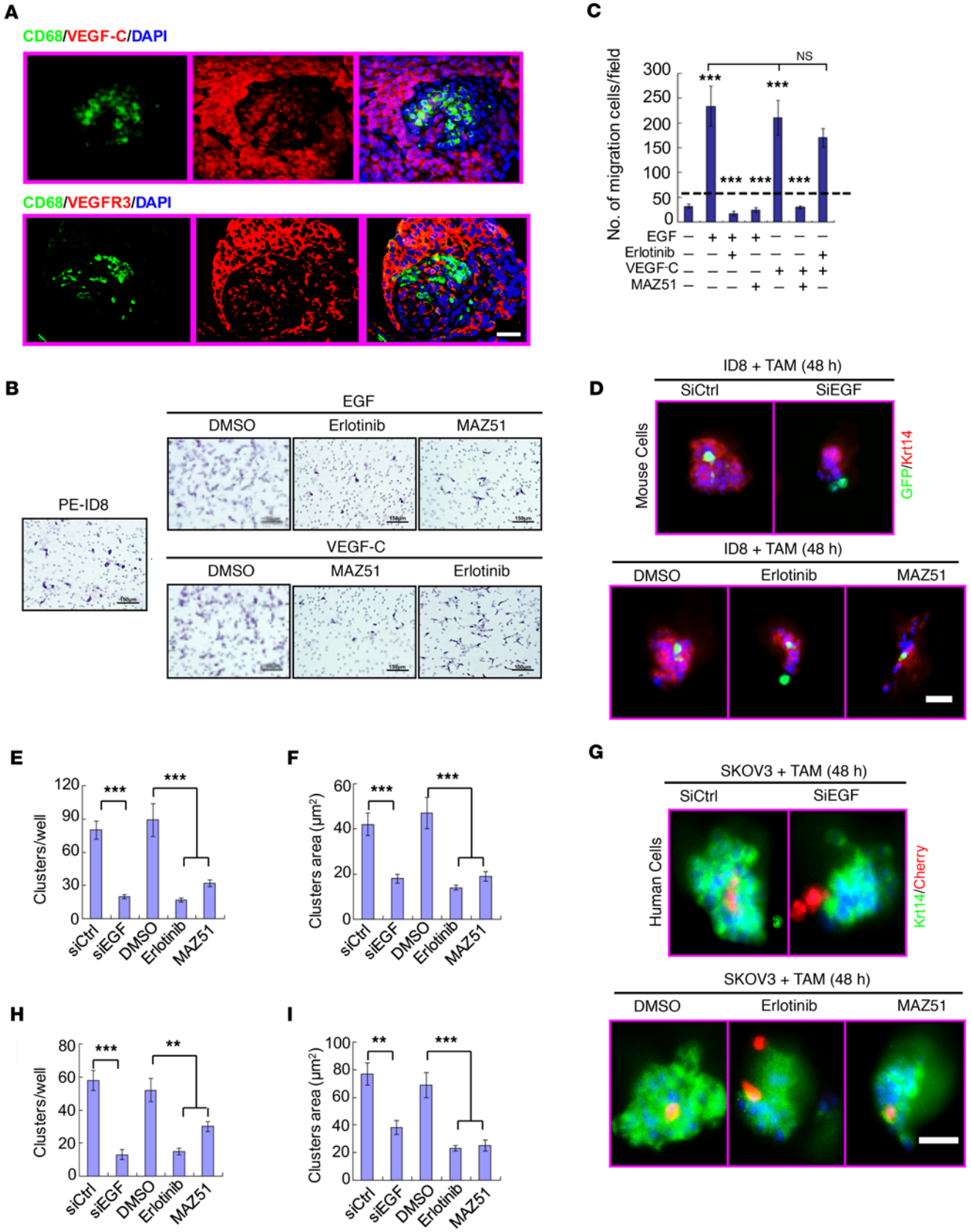
A
CD68/VEGF-C/DAPI
CD68/VEGFR3/DAPI
B
PE-ID8
EGF
DMSO
Erlotinib
MAZ51
VEGF-C
DMSO
MAZ51
Erlotinib
C
No. of migration cells/field
NS
***
EGF
Erlotinib
VEGF-C
MAZ51
D
ID8 + TAM (48 h)
SiCtrl
SiEGF
Mouse Cells
GFP/Krt14
ID8 + TAM (48 h)
DMSO
Erlotinib
MAZ51
E
Clusters/well
siCtrl
siEGF
DMSO
Erlotinib
MAZ51
F
Clusters area (μm²)
G
SKOV3 + TAM (48 h)
SiCtrl
SiEGF
Human Cells
Krt14/Cherry
SKOV3 + TAM (48 h)
DMSO
Erlotinib
MAZ51
H
Clusters/well
I
Clusters area (μm²)

Figure 7. EGF promotes EGFR$^+$ tumor cell migration through an autocrine VEGF-C/VEGFR3 signaling. (**A**) Immunofluorescent stainings of CD68 with VEGF-C or VEGFR3 in spheroids harvested from ascites of OC mice. Scale bar: 10 μm. Representative images of spheroids. n = 5 mice. (**B** and **C**) PE-ID8 cells were treated with EGF or VEGF-C (20 ng/ml) in the absence or presence of EGFR inhibitor erlotinib or VEGFR3 inhibitor MAZ51 (10 nM) for 12 hours during Transwell migration assay. (**B**) Representative images of hematoxylin staining. Scale bars: 150 μm. (**C**) Statistical analyses of migration cells. (**D**–**F**) Mouse GFP$^+$F4/80$^+$CD206$^+$ TAMs isolated from spheroids of OC-bearing tomato$^{LysM\text{-}Cre}$ mice were pretransfected with control siRNA (siCtrl) or EGF-siRNA for 48 hours. TAMs were then cocultured with ID8 cells in a 3D coculture system in the presence of erlotinib or MAZ51 (20 nM). Representative pictures are shown for localization of GFP$^+$ cells (TAMs) in the center of spheroids in control but not in siEGF cells. Number (per well) and size (area) of spheroids at 48 hours were quantified. Scale bars: 50 μm. (**G**–**I**) Human CD14$^+$ TAMs isolated from spheroids of OC patients were pretransfected with control siRNA or EGF-siRNA for 48 hours and applied to 3D coculture with human OC SKOV3 cells. Number and size of spheroids at 48 hours were quantified. Scale bar: 25 μm. Three different replicates were performed for all experiments. Data are presented as mean ± SEM. $^{**}P < 0.01$; $^{***}P < 0.001$ (2-sided Student's t test).

which TAMs promote OC migration, we first determined effects of F4/80$^+$CD206$^+$ TAMs on ID8 cells isolated from the spheroids in the peritoneal cavity (PE-ID8) in wound-healing and Transwell assays. F4/80$^+$CD206$^+$ TAMs, but not monocytes, significantly promoted PE-ID8 cell migration in both assays (Supplemental Figure 10, A–D). However, TAM-stimulated tumor migration was completely blunted by either the knocking down of EGF in TAMs or by treatment of ID8 with erlotinib (Supplemental Figure 10, E and F). These results suggest that the reciprocal upregulation of EGF in TAMs and EGFR in tumor cells is critical for TAM-promoted ovarian tumor cell migration.

It has been reported that VEGF-C/VEGFR3 signaling promotes tumor cell migration in a lung cancer model (19). We observed high levels of VEGFR3 on ID8 cells. Interestingly, we detected VEGF-C in PE-ID8, but not in naive ID8 cells or TAMs (Supplemental Figure 11, A and B). Further immunostaining results confirmed that VEGF-C and VEGFR3 were highly expressed in ID8 tumor cells, but not in TAMs within the spheroids (Figure 7A). Immunoblotting analyses revealed that there were increased levels of VEGF-C and phosphorylated VEGFR3 in PE-ID8 as compared with unactivated ID8 cells (Supplemental Figure 11, C and D). We reasoned that EGF induced VEGF-C expression, which in turn activated VEGFR3 in tumor cells. Indeed, *VEGFC* levels were significantly increased in both mouse ID8 and human SKOV3 OC cells upon EGF treatment for 8 hours or longer, as determined by qRT-PCR (Supplemental Figure 11, E and F) and Western blot (Supplemental Figure 11, G and H); this induction was blocked by an EGFR inhibitor or an ERK/2 inhibitor (Supplemental Figure 11I). Consistently, VEGFR3 was phosphorylated upon either EGF or VEGF-C treatment, and such activation was abrogated by the EGFR inhibitor erlotinib or the VEGFR3 inhibitor MAZ51. However, the EGFR inhibitor could not block the activation of VEGFR3 induced by VEGF-C (Supplemental Figure 11J), suggesting that EGF/EGFR signaling functions upstream of VEGF-C/VEGFR3 signaling. Functionally, both EGF and VEGF-C could promote ID8 cell migration. Consistent with the signaling results, the VEGFR3 inhibitor blocked both EGF- and VEGF-C–induced ID8 cell migration (Figure 7, B and C). These results suggest a critical role of the EGF/EGFR/VEGF-C/VEGFR3 signaling pathway in regulating OC cell migration.

Finally, we determined how TAMs facilitate spheroid formation. To this end, we established an in vitro spheroid formation assay using a standard 3D coculture system. Human CD14$^+$ TAMs and mouse GFP$^+$F4/80$^+$CD206$^+$ TAMs isolated from spheroids of OC-bearing donor tomato$^{LysM\text{-}Cre}$ mice were mixed with ID8 cells (TAM:ID8 at a ratio of 1:10) in medium containing 2% Matrigel and seeded onto the 24-well plate precoated with Matrigel. In this model, we detected spheroid formation at 48 hours of coculture. As we observed in vivo, GFP$^+$CD68$^+$ TAMs were localized in the center of clusters surrounded by tumor cells as visualized by keratin-14, E-cadherin, and β-catenin staining (Supplemental Figure 12A). To confirm whether tumor cell migration is required for spheroid formation, we tested effects of EGF siRNA in TAMs and EGFR- or VEGFR3-specific inhibitors on spheroids in the 3D coculture. KD of EGF in TAMs and inhibition of EGFR or VEGF-C/VEGFR3 signaling drastically reduced the number and size of spheroids in the mouse cell 3D coculture system (Figure 7, D–F, and Supplemental Figure 12B). More importantly, similar results were obtained for the 3D coculture system using human TAMs isolated from OC patients and SKOV3 cells (Figure 7, G–I). We detected viable dispersed TAMs and small tumor cell clusters in EGF-KD, EGFR inhibitor, and VEGFR3 inhibitor groups (Figure 7, D and G, and Supplemental Figure 12A), indicating that associations of TAMs with tumor cells were blocked upon inhibition of EGF/EGFR and VEGF-C/VEGFR3 signaling.

EGF promotes adhesion of EGFR$^+$ tumor cells with TAMs through ICAM-1–$\alpha_M\beta_2$ integrin interaction. We reasoned that adhesions of tumor cells to TAM are required for spheroid formation. It is reported that TAMs in spheroids provide integrins to support adhesions of tumor cells (20). We therefore screened the expression pattern of various integrins in TAMs and ID8 ovarian tumor cells isolated from the peritoneal cavity (PE-ID8) by qRT-PCR. Integrin β_2 was highly expressed in spheroid-associated F4/80$^+$CD206$^+$ TAMs, but not in spheroid tumor cells (Supplemental Figure 13A). Expression of leukocyte-specific integrins *Cd11b* (integrin α_M) and *Cd11c* (integrin α_X), but not *Cd11a* (integrin α_L), were detected in the TAMs (Supplemental Figure 13A). FACS analysis also showed that CD11b and CD11c were highly induced in TAMs (Supplemental Figure 13, B and C). CD11b and CD11c associated with integrin β_2 to form macrophage-1 (Mac-1) and inactivated C3b receptor 4 (CR4), respectively. These integrins can bind to similar ligands ICAM-1 or ICAM-2 on vascular endothelium during extravasation to inflammatory tissues (21). We examined expression of *Icam1* and *Icam2* within spheroids and found ICAM-1, but not ICAM-2, was highly expressed in the spheroids as detected by qRT-PCR (Supplemental Figure 14A). We then determined which cell types expressed ICAM-1 within the spheroids by immunostaining. To our surprise, ICAM-1 was highly expressed in ID8 tumor cells, but not in TAMs (Figure 8A). The basal level of ICAM-1 in naive ID8 cells was very low, but was drastically upregulated by EGF at both mRNA and protein levels (Supplemental Figure 14, B–D). EGF-induced ICAM-1 expression was abrogated by EGFR- or ERK1/2

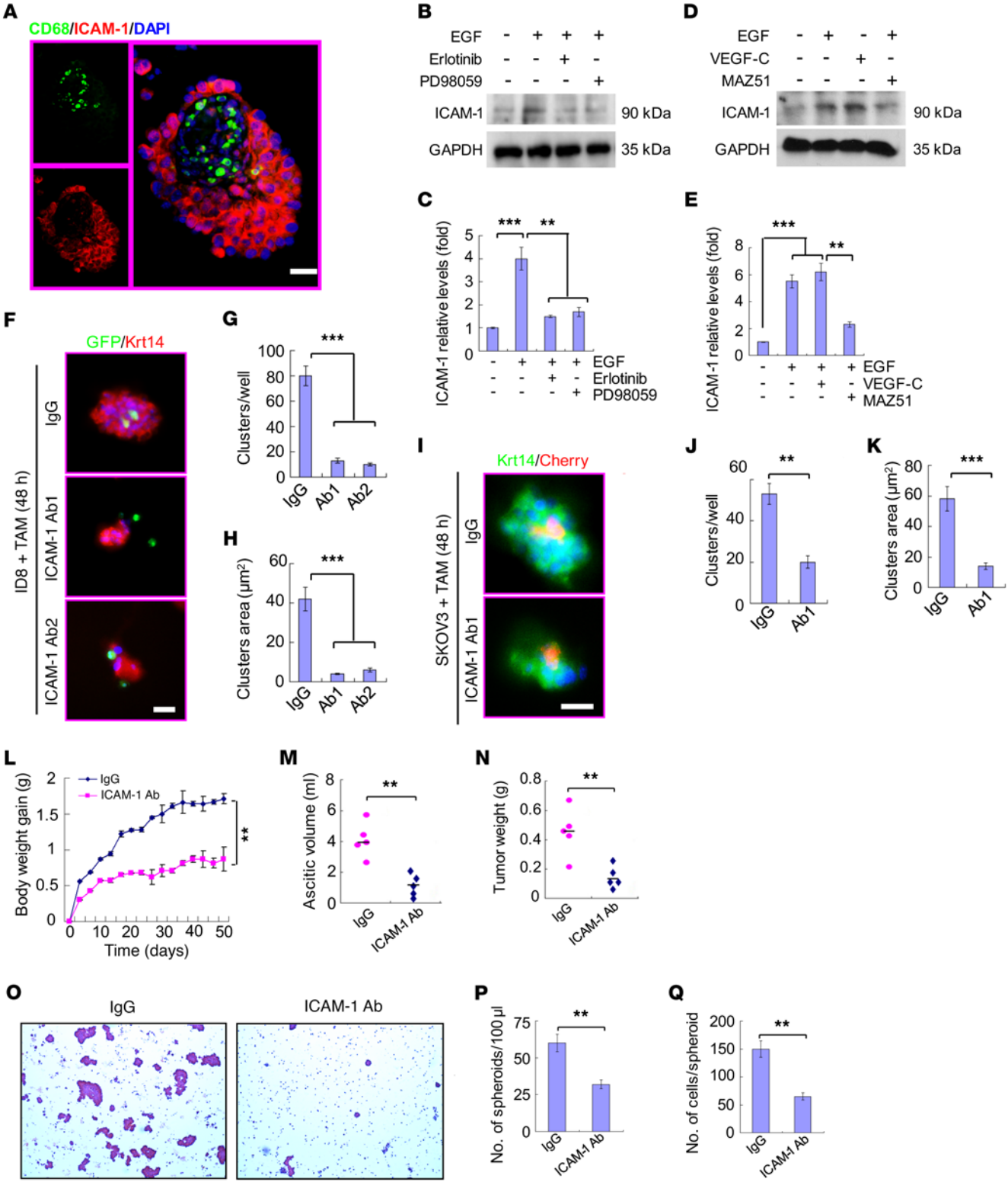
A
CD68/ICAM-1/DAPI
B
EGF
Erlotinib
PD98059
ICAM-1
GAPDH
90 kDa
35 kDa
D
EGF
VEGF-C
MAZ51
ICAM-1
GAPDH
90 kDa
35 kDa
C
ICAM-1 relative levels (fold)
EGF
Erlotinib
PD98059
E
ICAM-1 relative levels (fold)
EGF
VEGF-C
MAZ51
F
GFP/Krt14
ID8 + TAM (48 h)
IgG
ICAM-1 Ab1
ICAM-1 Ab2
G
Clusters/well
IgG
Ab1
Ab2
H
Clusters area (μm²)
IgG
Ab1
Ab2
I
Krt14/Cherry
SKOV3 + TAM (48 h)
IgG
ICAM-1 Ab1
J
Clusters/well
IgG
Ab1
K
Clusters area (μm²)
IgG
Ab1
L
IgG
ICAM-1 Ab
Body weight gain (g)
Time (days)
M
Ascitic volume (ml)
IgG
ICAM-1 Ab
N
Tumor weight (g)
IgG
ICAM-1 Ab
O
IgG
ICAM-1 Ab
P
No. of spheroids/100 μl
IgG
ICAM-1 Ab
Q
No. of cells/spheroid
IgG
ICAM-1 Ab

Figure 8. TAMs promote adhesion with EGFR$^+$ tumor cells through integrin $\alpha_M\beta_2$ and ICAM-1 interaction. (**A**) Immunofluorescent stainings of CD68 with ICAM-1 in spheroids harvested from ascites of OC mice. Representative images of spheroids from n = 5 mice are shown. Scale bar: 10 μm. (**B** and **C**) PE-ID8 cells were treated with EGF in the absence or presence of EGFR inhibitor erlotinib or ERK inhibitor PD98059 (10 nM) for 24 hours. ICAM-1 protein was determined by Western blot. Relative levels of ICAM-1 were quantified. (**D** and **E**) ID8 cells were treated with EGF or VEGF-C in the absence or presence of MAZ51 (VEGFR3 inhibitor) for 24 hours. ICAM-1 was determined by Western blot (**D**). Relative protein levels of ICAM-1 were quantified (**E**). (**F**–**K**) Effects of ICAM-1 neutralization antibodies on spheroid formation. 3D cocultures of mouse TAM–ID8 (**F**–**H**) and human TAM-SKOV3 (**I**–**K**) were performed as in Figure 7 in the presence of anti-mouse ICAM-1 or anti-human ICAM-1, respectively. Number and size of spheroids were measured at 48 hours. Scale bars: 50 μm (**F**); 25 μm (**I**). Three independent experiments were performed. Data are presented as mean ± SEM. $^{**}P < 0.01$; $^{***}P < 0.001$. (**L**–**Q**) An orthotopic mouse model was established by injecting mouse ID8 OCs i.p. into C57BL/6 female recipient mice. Mice were then either treated with IgG or anti-mouse ICAM-1 antibody by i.p. injection. Mouse body weight gain was measured at indicated time points (days 0–50) (**L**). Ascetic volume (**M**) and tumor weight (**N**) were measured at day 50. (**O**–**Q**) Spheroids were examined by H&E staining (**O**). Total number (**P**) and size (**Q**) of spheroids were quantified. Data are presented as mean ± SEM. n = 10. $^{**}P < 0.001$ (2-sided Student's t test).

inhibitors (Figure 8, B and C). Interestingly, EGF-induced ICAM-1 expression was also blocked by a VEGFR3 inhibitor. Consistently, VEGF-C induced ICAM-1 expression in ID8 cells (Figure 8, D and E, Supplemental Figure 14, E–G). Similarly to the mouse data, integrin $\alpha_M\beta_2$ was highly expressed in TAMs, while VEGF-C/VEGFR3 and ICAM-1 were highly expressed in peritoneal spheroids of OC patients. Moreover, there was a positive correlation between EGF and VEGF-C expression (Supplemental Figure 15, A–C).

We next tested to determine whether interactions between integrins on TAMs and ICAM-1 on tumor cells were critical for initial spheroid formation. To this end, we employed various neutralization antibodies in the 3D spheroid formation assays. A neutralization antibody of CD11b, CD11c, and integrin β_2, but not of CD11a or a control IgG, significantly reduced the number and size of spheroids formed by mouse TAMs and ID8 cells (Supplemental Figure 16, A–C). More importantly, a combination of anti-CD11b / anti-CD11c or anti-CD11b/anti-CD11c/anti–integrin β_2 more dramatically blocked the spheroid formation (Supplemental Figure 16, A–C). We also observed that ICAM-1 neutralization antibodies, but not control IgGs, significantly decreased the number and the size of spheroids in the 3D coculture systems using both mouse (Supplemental Figure 16D and Figure 8, F–H) and human cells (Figure 8, I–K). These data support an important role of the association between the CD11b/c–integrin β_2 complex on TAMs and the ligand ICAM-1 on OC cells in spheroid formation.

To explore therapeutic effects of ICAM-1 neutralization antibodies for treatment of OC, ID8 tumor–bearing mice were treated with anti–ICAM-1 antibodies or control IgGs in the established orthotopic mouse model. Phenotype analyses showed that the anti–ICAM-1 antibody group significantly reduced mouse total body weight, ascitic fluid volume, and wet weight of tumor cells isolated from the ascitic fluid (Figure 8, L–N). Similarly to effects of EGFR inhibitors, the number and size of spheroids were significantly reduced by anti–ICAM-1 antibodies (Figure 8, O–Q). These results suggest that integrin–ICAM-1–mediated TAM-tumor associations play a critical role in spheroid formation and transcoelomic metastasis of OC.

Discussion

Transcoelomic (peritoneal) metastasis occurs in nearly all patients with OC (more than 90%), especially at late stages, causing death (22). Transcoelomic metastases also can happen in many other cancers, such as pancreatic (50%) and colon cancers (32%) (23). Therefore, study of the common mechanism for transcoelomic metastasis is critical for improving the prognosis of OC patients as well as other transcoelomic metastatic cancers. Considering the unique characteristics of the peritoneum, such as its large area and lack of blood supply and lymphatic vessels, it is puzzling how detached OC cells obtain the necessary matrix support to avoid anoikis, are protected against immune cell attack, and have access to specific growth factors to maintain their rapid growth and implantation. It has been reported that OC cells can upregulate survival pathways such as activation of RAB25 to gain anchorage-dependent survival, while upregulating surface immunosuppressor molecules (e.g B7-H4 and complement C1 inhibitor) to escape attacks by the immune system (e.g., T cell or the complement) (24, 25). Spheroid formation is another essential step in the initiation of peritoneal implantation metastasis for OC. However, a detailed mechanism for spheroid formation remains unknown (20, 26, 27). Through the analysis of cell components in spheroids isolated from ascites of 128 cases of stage III OC patients, we observed that macrophages presented in all the spheroids. Moreover, we noticed that the number of macrophages in spheroids in ascites was substantially more than that in primary tumors. In addition, we found the number of macrophages was positively associated with proliferation in spheroid, but negatively associated with the prognosis of OC patients. Our results suggest that spheroid-associated TAMs may play an important role in human OC progression.

TAMs in solid tumors can promote tumor angiogenesis and cancer metastasis through the secretion of proangiogenic factors and chemoattractants. TAMs also secret cytokines to promote tumor premetastatic niche formation (28–41). The role of macrophages in OC has been previously investigated in mouse models. Robinson-Smith et al. reported that the risk for peritoneal implantation of OC is increased when intraperitoneal inflammation is enhanced; depletion of peritoneal macrophages, but not neutrophils and natural killer cells, reduces the chance of peritoneal metastasis (42). These results and our observations from human samples have prompted us to hypothesize that macrophages may play a critical role in spheroid formation before peritoneal implantation. This hypothesis is strongly supported by our intriguing discovery that TAMs are located in the center of spheroids in both human and mouse OC samples (Figure 9A). We have further provided strong evidence that TAMs are essential at the initiation step of spheroid formation. In an orthotopic OC model using *GFP*-transgenic recipient mice, we observed that nearly 80% of macrophages infiltrated into the peritoneal cavity were detected in spheroids. The size and number of spheroids was markedly reduced when TAMs were deprived by clodronate

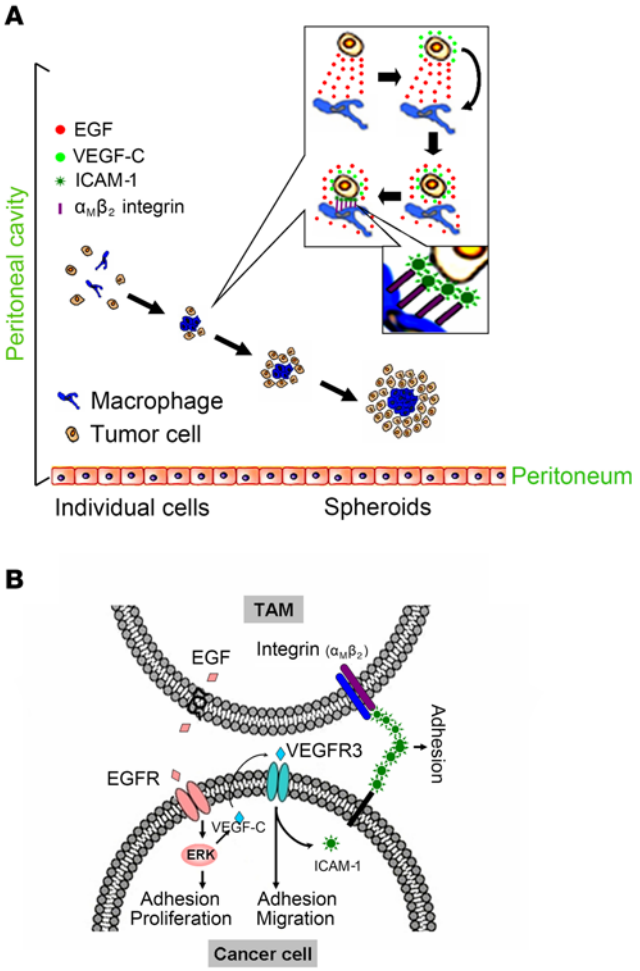

Figure 9. A model for TAM–cancer cell interactions in spheroid formation. (**A**) During early stages of OC transcoelomic metastasis and tumor growth, detached OC cells induce infiltration of macrophages into the peritoneal cavity. Interactions of macrophages with OC cells in the peritoneal environment form spheroids and skew macrophages into M2 subtype TAMs. TAMs located in the center of spheroids may provide initial matrix support for OC to avoid anoikis. Importantly, TAMs can secrete large amount of EGF and activate EGFR that is upregulated on tumor cells. The activated EGF/EGFR signaling can induce VEGF-C expression, which in turn activates VEGFR3 signaling and induces integrin/ICAM-1 expression in tumor cells to form a positive autocrine feedback loop, thus promoting tumor migration, adhesion, and spheroid formation. (**B**) Molecular interactions between TAMs and OC cells.

treatment. In turn, peritoneal implantation was inhibited and survival time was prolonged. Conversely, the size and number of spheroids was substantially increased when isolated TAMs were injected into the peritoneal cavity of the mice. Interestingly, macrophages infiltrated into the peritoneal cavity gradually gained an M2-like phenotype. The TAM polarization may be triggered by the peritoneal microenvironment (such as hypoxia and metabolites) as observed in solid tumors (34–38, 43). Importantly, we have defined the mechanism by which TAMs facilitate OC cell adhesion and spheroid formation. It is known that adhesion is a necessary factor for spheroid formation, and studies have suggested that free cells detached from the primary tumor may form spheroids through the interaction between $\alpha_5\beta_1$ integrin and fibronectin (20). In solid tumors, adhesion of tumor cells to the matrix is usually involved in cancer metastasis (44). However, not much is known about the adhesion of OC cells with TAMs in spheroid formation. We discovered, as we expected, that spheroid-associated OC cells express ICAM-1, a ligand known to bind to integrins CD11b and CD11c on macrophages. Moreover, ICAM-1 neutralization antibodies completely diminish the spheroid formation of both mouse and human TAM-OC cells in the in vitro 3D coculture models. Most importantly, blockade of CD11b/c–ICAM-1 interaction by ICAM-1 neutralization antibodies attenuated spheroid formation and OC progression in vivo. Of note, it has been reported that increased tumor $CD45^+CD33^+$ MDSC numbers are a significant and independent predictor of poor survival in OC; MDSCs enhance cancer stem cell gene expression, spheroid formation, and cancer metastasis in OC models in vivo (45). It needs to be determined whether MDSCs play role in spheroid formation similar to that of TAMs.

In the OC mouse models, we observed that an increase in tumor cell number at 3 weeks after implantation was correlated with formation of tumor spheroids. Indeed, TAM-associated spheroids exhibited enhanced tumor cell proliferation in mouse models and human OC samples. Moreover, TAMs could directly promote proliferation of tumor cells by in vitro Transwell assays, suggesting that TAMs regulate tumor growth through releasing certain regulatory factors. By screening a panel of growth factors and their cognate receptors in TAMs and spheroid-associated tumor cells, we have identified the EGF/EGFR regulatory pathway that is critical for TAM-stimulated OC proliferation and cancer progression. A previous study reported that EGFR expression increased significantly in free tumor cells compared with implanted tumor cells in the peritoneal cavity, suggesting that the EGFR pathway plays an important role in peritoneal free tumor cells (46). It is well known that the peritoneal cavity contains abundant macrophages and T lymphocytes in the ascites of OC patients (47). Moreover, it has been reported that EGF from macrophage promotes invasion of breast carcinoma cells (48). Our study clearly demonstrates that TAM is the major source of EGF, which induces EGFR-positive OC proliferation, as demonstrated by EGF KD and EGFR inhibitor in in vitro and mouse models. It needs to be determined how EGF in TAMs is regulated in the peritoneal cavity microenvironment. It is likely that TAM–OC cell interactions in spheroids enhance EGF expression. Similarly, EGFR was markedly upregulated in spheroid-associated OC cells isolated from ascites. Intriguingly, EGFR-positive OC cells surrounded EGF-positive TAMs in the spheroids. This close proximity suggests that TAMs in the center of spheroids not only provide initial matrix support for OC to avoid anoikis, but also facilitate OC cell proliferation through the EGF-EGFR paracrine loop. Furthermore, we demonstrate that the EGF/EGFR axis is not only critical for proliferation of OC, but also induces expression of VEGF-C in OC cells, which in turn activates the VEGFR3 autocrinal pathway to enhance integrin/ICAM-1 expression, OC cell migration, and spheroid formation (Figure 9B). This conclusion is based on the following observations: (a) the proliferation of OC cells was substantially blocked upon EGF KD or treatment with the EGFR inhibitor erlotinib in a Transwell coculture with TAMs. Moreover, the EGFR inhibitor erlotinib drastically retarded spheroid formation, OC cell proliferation, and tumor

growth in 2 mouse OC models. (b) TAM-produced EGF induced expression of VEGF-C in the OC cell, which in turn activated the VEGFR3 pathway; EGF-induced VEGF-C in the OC cell could be abrogated by inhibition of EGFR-ERK signaling. Importantly, both EGF and VEGF-C stimulated expression of ICAM-1 in the OC cell and OC cell migration; all of these effects could be diminished by VEGFR3 inhibitors. Therefore, VEGF-C/VEGFR3 acts downstream of EGFR signaling in OC cells (Figure 9B).

Our data indicate that depletion of TAMs or blockade of EGFR in OC cells by erlotinib at an early stage, but not at late stages, effectively inhibits the transcoelomic metastasis of OC. Our study may provide an explanation of why anti-EGF single-agent therapy has not been successful in advanced OC patients (17, 18). Therefore, early diagnosis, depletion of TAMs, and anti-EGF therapy are needed for the treatment of OC. Furthermore, our model showing that EGF/EGFR signaling, VEGF-C/VEGFR3 signaling, and ICAM-1–integrin CD11b/c association are required for OC cell proliferation, migration, adhesion, and spheroid formation is of clinical significance. Therefore, ICAM-1 neutralization antibodies, similar to blockade of EGF and VEGFR3 signaling, strongly inhibit spheroid formation in vitro. Moreover, ICAM-1 neutralization antibodies profoundly reduce the number and size of spheroids and tumor progression in mouse models. Our data suggest that neutralization of ICAM-1 may provide novel therapeutics for the treatment of OC.

Taken together, our study demonstrates that TAMs play an essential role in spheroid formation during the process of transcoelomic metastasis of OC. TAM can secrete large amounts of EGF to activate EGFR in surrounding tumor cells. The activated EGF/EGFR signaling can upregulate VEGF-C, which in turn upregulates integrins and ICAM-1 to form a positive autocrine feedback loop, thus promoting tumor cell proliferation, migration, adhesion, spheroid formation, and peritoneal implantation (Figure 9B). Our current study has unveiled the underlying mechanism of spheroid formation, providing a strategy for inhibiting implantation metastasis and improving the prognosis of OC patients.

Methods

Animal model. All mice were maintained on a C57BL/6 background. *LysM-Cre* mice were crossed with tomato reporter (*mT/mG*) mice to lineage label lysozyme-derived cells. Nude mice were purchased from The Jackson Laboratory. Mouse OC ID8 or human OC SKOV3 cells (1×10^6/ml) were injected into the abdominal cavities of C57BL/6 background or nude mice in 100 μl of DMEM. Mouse body weight gain, ascitic fluid volume, and tumor weight were measured by electronic balance. The mice were sacrificed after 9 weeks, and the tumor spheroids and tumor implantations were analyzed by histology.

In vivo treatment in mouse models. Mice were divided into groups of 10. An orthotopic mouse model was established by injecting mouse ID8 OCs i.p. into C57BL/6 female recipient mice. For LC treatment, LC was administrated s.c. at 10 μl/g body weight every 4 days (except 20 μl/g at the first dose). For EGFR inhibitor treatment, erlotinib was injected i.p. at 100 mg/kg body weight/d. For antibody treatment, mice were injected i.p. with normal rat IgG or rat anti-ICAM1 antibody (5 mg/kg, 1 time/3 d). Experimental and control mice were killed at 50 days after tumor cells were injected. Ascites and spheroids were collected for H&E staining and FACS.

Clinical samples. Following Institutional Review Board approval, a total of 128 patients with advanced epithelial OC (EOC) from the research files at The Tumor Affiliated Hospital of Harbin Medical University who were seen from January 2005 to December 2009 and who met our inclusion criteria were entered in this study. The eligibility criteria included the following: (a) pathologic examination confirming the presence of stage III EOC; (b) complete basic clinical data; (c) absence of any prior treatment for cancer; (d) no serious complications or other malignant disease; and (e) the patients and family members having been informed about the illness and given informed consent before treatment. All patients had undergone complete cytoreductive surgery. Human tumor spheroids from advanced stage (i.e., stages III–IV) OC patients were harvested from consenting patients for ascitic fluid collection (Human Investigation Committee (HIC) protocol #1111003959; http://your.yale.edu/research-support/human-research).

Cell culture. The ID8 (mouse EOC line) was a gift from Jack Lawler and Carmelo Nucera at Beth Israel Deaconess Medical Center (Harvard Medical School, Boston, Massachusetts, USA) (49). SKOV3 cells (human ovarian adenocarcinoma cell line) were obtained from ATCC. SKOV3 cells are resistant to tumor necrosis factor and to several cytotoxic drugs, including diphtheria toxin, cisplatinum, and adriamycin. ID8 and SKOV3 cells were cultured in DMEM (Life Technologies) supplemented with 10% FBS, 100 U/ml penicillin, and 100 μg/ml streptomycin at 37°C in a humidified atmosphere of 5% CO_2 and 95% air. The culture medium was changed every 2 days, and cells were split when they reached 80%–90% confluence. For all experiments, cells were seeded at an appropriate density and grew to 80%–90% confluence before experimentation. Primary mouse TAMs and PE-ID8 cells were isolated from the peritoneal cavity after i.p. injection of ID8 cells for different time points in C57BL/6 background mice.

Recombinant protein and inhibitors. Recombinant human and mouse EGF and VEGF-C were purchased from R&D Systems. MAZ51 (VEGFR3 inhibitor) was purchased from EMD Millipore. Erlotinib (EGFR inhibitor) was purchased from Roche. Clophosome–neutral LC for macrophage depletion was purchased from FormuMax Scientific Inc. (product code F70101-N).

Immunostaining. Antibodies used for immunohistochemistry and immunofluorescent staining are listed in the Supplemental Information (Supplemental Table 4). Confocal microscopy images were taken with a Zeiss-LSM 700 microscope and evaluated using ZEN2010 software. For mean fluorescence intensity measurements, confocal microscopy images were analyzed with ImageJ (NIH). Slides were observed using a Zeiss Axiovert 200 fluorescence microscope (Carl Zeiss MicroImaging), and images were captured using Openlab3 software (Improvision). For tissue, 5-μm serial sections cut from frozen, OCT-embedded tissues were fixed in –20°C acetone for 10 minutes and dried for 15 minutes, followed by the same blocking/antibody protocol for cells as listed above. Additional details are available in the Supplemental Information.

Protein extraction and Western blot analysis. Freshly dissected unfixed tissue was homogenized in lysis buffer. The lysates were centrifuged at 13,000 *g* for 10 minutes at 4°C. Supernatants were collected and protein concentration was determined with a Bradford Protein Assay kit (Bio-Rad). The cell lysates were subjected to SDS-PAGE, followed by immunoblotting (Immobilon P; Millipore) with specific antibodies, followed by detection using an enhanced

chemiluminescence kit (Amersham; GE Healthcare Life Sciences). All antibodies used for Western blotting are listed in the Supplemental Information.

FACS. Analyses of mouse cell surface CD11b, F4/80, CD3e, CD206, and CD163 and human cell surface CD14 and CD326 expression by FACS were described previously (12–15, 50). Briefly, mouse TAM suspensions were stained with mouse CD11b-FITC, F4/80-PE, CD3e-APC, PE-CD206, and APC-CD163 and human CD14, CD326 antibodies for 15 minutes on ice. Isotype antibody served as a negative control. Flow cytometry was performed on a FACSCalibur (BD Biosciences). Data were analyzed with BD CellQuest Pro software. All antibodies used for FACS are listed in Supplemental Information.

Migration assay. The migration activity of macrophages and tumor cells was demonstrated using the Transwell cell culture system (Corning; pore size, 0.3 or 8 μm) in vitro. To test the migration assays of ID8 cells, 1×10^{-4} ID8 cells were seeded on the upper surface of the Transwell chamber. Different chemoattractants (VEGFC or EGF) or macrophages (TAM) were placed in the lower chamber. After 12 hours of incubation, ID8 cells on the upper face of the Transwell membrane were removed with a cotton swab. The cells on the bottom surface of the Transwell membrane were then fixed in 4% PFA and stained with H&E. Migrated cells were counted in 5 randomly chosen fields under a microscope (200×).

qRT-PCR. Total RNA was extracted from human tissues using the RNeasy Plus Mini Kit (74134, QIAGEN) and then converted into cDNAs using the High Capacity cDNA Reverse Transcription Kit (4368814, Applied Biosystems) following the manufacturer's instructions. Quantitative PCR was performed with a CFX-96 (Bio-Rad) using the RT2 SYBR Green Kit 330500, SA Biosciences). All primers used for qRT-PCR are listed in the Supplemental Information (Supplemental Table 5). All values were normalized with *Gapdh* abundance. Data were presented as the average of triplicates ± SD.

3D coculture system of TAM and ID8 cells. Mouse F4/80$^+$CD206$^+$ TAMs were isolated by FACS sorting from spheroids of OC-bearing donor tomato$^{LysM\text{-}Cre}$ mice. Human tumor spheroids from advanced-stage (i.e., stages III–IV) OC patients were harvested (HIC protocol #1111003959) (51) followed by FACS identification and sorting for CD14$^+$ TAMs (12–15, 50). The 24-well plates were precoated with Matrigel as described above. The mixtures of TAMs and ID8 cells (at a ratio of 1:10 but with a fixed total cell number of 40,000 cells/well) were directly seeded onto the Matrigel-precoated 24-well plate. The cells were incubated at 37°C for up to 48 hours to allow the aggregates/spheroids to form. EGFR inhibitor erlotinib, VEGFR3 inhibitor MAZ51 (20 nM each), or anti–ICAM-1 antibody (20 μg/ml) was added at 6 hours after coculture. Fluorescent microscopic images were taken to analyze the morphology at from 6 to 48 hours. The wells without cells but containing medium were used as a negative control. All assays were performed at least 3 times and tested in triplicate each time. All microscopic images were observed using the Zeiss Axiovert 200 fluorescence microscope (Carl Zeiss MicroImaging), and images were captured using Openlab3 software (Improvision) (14, 15).

Statistics. The differences in results of Western blot, qRT-PCR, cell-proliferation assays, immunostainings, FACS, and tumor growth were analyzed by Student's t test. The differences in demographic characteristics of OC patients were analyzed by χ^2 or Fisher's exact test. The Kaplan-Meier method was used to estimate OS, while the differences in the levels among possible prognostic factors were compared by the log-rank test with univariate analyses. A multivariate Cox regression (proportional hazard model) was employed to identify prognostic factors and evaluate the independent impact of CD68 levels on OS. Statistical analyses in this study were performed using SAS software (version 9.1.4, SAS Institute). All statistical tests were 2 tailed, and P values of less than 0.05 were considered statistically significant.

Study approval. All animal studies were approved by the Institutional Animal Care and Use Committee of Yale University. Human tumor spheroids from advanced-stage (i.e., stages III–IV) OC patients were harvested from consenting patients for ascitic fluid collection at Yale University School of Medicine (HIC protocol #1111003959). Clinical paraffin samples were approved by the Institutional Review Board at The Tumor Affiliated Hospital of Harbin Medical University.

Additional methods see Supplemental Experimental Procedures in the Supplemental Information.

Author contributions

MY, XL, ST, HJZ, SB, XX, and HZ performed experiments. GL provided human samples. SB and ADS provided human OC–associated macrophages. MY and WM designed and analyzed experiments and wrote the manuscript. WJ and ADS edited the manuscript.

Acknowledgments

We thank Katerina Politi for discussion. This work was partly supported by National Key Research and Development Program of China (2016YFC1300600), National Natural Science Foundation of China (No. 91539110) and Scientific Grants of Guangdong (No. 2015B020225002 and 2015A050502018) to WM; NIH grants R01 HL109420 and HL115148 to WM; NIH grants R01 CA154460-01 and U01 CA176067-01A1 to ADS.

Address correspondence to: Wang Min, Center for Translational Medicine, The First Affiliated Hospital, Sun Yat-sen University, 58 Zhongshan Er Road, Guangzhou, 510080, China; or to: Interdepartmental Program in Vascular Biology and Therapeutics, Department of Pathology, Yale University School of Medicine, 10 Amistad Street, 401B, New Haven, Connecticut 06520, USA. Phone: 203.785.6047; E-mail: wang.min@yale.edu. Or to: Ge Lou, Department of Gynecology, The Tumor Affiliated Hospital of Harbin Medical University, Harbin 150086, China. Phone: 86-451-86298303; E-mail: yinlouge@126.com.

1. Jemal A, Siegel R, Ward E, Hao Y, Xu J, Thun MJ. Cancer statistics, 2009. *CA Cancer J Clin*. 2009;59(4):225–249.
2. Siegel R, Naishadham D, Jemal A. Cancer statistics, 2012. *CA Cancer J Clin*. 2012;62(1):10–29.
3. Rossing MA, Wicklund KG, Cushing-Haugen KL, Weiss NS. Predictive value of symptoms for early detection of ovarian cancer. *J Natl Cancer Inst*. 2010;102(4):222–229.
4. Yin M, et al. Over-expression of LAPTM4B is associated with poor prognosis and chemotherapy resistance in stages III and IV epithelial ovarian cancer. *J Surg Oncol*. 2011;104(1):29–36.
5. Yin M, et al. LAPTM4B overexpression is a novel predictor of epithelial ovarian carcinoma metastasis. *Int J Cancer*. 2011;129(3):629–635.
6. Dusenbery KE, Bellairs EE, Potish RA, Twiggs LB, Boente MP. Twenty-five year outcome of sequential abdominal radiotherapy and melphalan:implications for future management of epithelial carcinoma of the ovary. *Gynecol Oncol*.

2005;96(2):307–313.
7. Omura GA, et al. Long-term follow-up and prognostic factor analysis in advanced ovarian carcinoma: the Gynecologic Oncology Group experience. *J Clin Oncol*. 1991;9(7):1138–1150.
8. Tan DS, Agarwal R, Kaye SB. Mechanisms of transcoelomic metastasis in ovarian cancer. *Lancet Oncol*. 2006;7(11):925–934.
9. Peart T, et al. Intact LKB1 activity is required for survival of dormant ovarian cancer spheroids. *Oncotarget*. 2015;6(26):22424–22438.
10. Rafehi S, et al. TGFβ signaling regulates epithelial-mesenchymal plasticity in ovarian cancer ascites-derived spheroids. *Endocr Relat Cancer*. 2016;23(3):147–159.
11. Zhang Y, et al. A network of interactions enables CCM3 and STK24 to coordinate UNC13D-driven vesicle exocytosis in neutrophils. *Dev Cell*. 2013;27(2):215–226.
12. Duraiswamy J, Freeman GJ, Coukos G. Therapeutic PD-1 pathway blockade augments with other modalities of immunotherapy T-cell function to prevent immune decline in ovarian cancer. *Cancer Res*. 2013;73(23):6900–6912.
13. Motz GT, Coukos G. Deciphering and reversing tumor immune suppression. *Immunity*. 2013;39(1):61–73.
14. Hagemann T, et al. Ovarian cancer cells polarize macrophages toward a tumor-associated phenotype. *J Immunol*. 2006;176(8):5023–5032.
15. Ko SY, Ladanyi A, Lengyel E, Naora H. Expression of the homeobox gene HOXA9 in ovarian cancer induces peritoneal macrophages to acquire an M2 tumor-promoting phenotype. *Am J Pathol*. 2014;184(1):271–281.
16. Tang PC, et al. MyD88-dependent, superoxide-initiated inflammation is necessary for flow-mediated inward remodeling of conduit arteries. *J Exp Med*. 2008;205(13):3159–3171.
17. Vergote IB, et al. Randomized phase III study of erlotinib versus observation in patients with no evidence of disease progression after first-line platin-based chemotherapy for ovarian carcinoma: a European Organisation for Research and Treatment of Cancer-Gynaecological Cancer Group, and Gynecologic Cancer Intergroup study. *J Clin Oncol*. 2014;32(4):320–326.
18. Pujade-Lauraine E, et al. Bevacizumab combined with chemotherapy for platinum-resistant recurrent ovarian cancer: The AURELIA open-label randomized phase III trial. *J Clin Oncol*. 2014;32(13):1302–1308.
19. Su JL, et al. The VEGF-C/Flt-4 axis promotes invasion and metastasis of cancer cells. *Cancer Cell*. 2006;9(3):209–223.
20. Casey RC, et al. Beta 1-integrins regulate the formation and adhesion of ovarian carcinoma multicellular spheroids. *Am J Pathol*. 2001;159(6):2071–2080.
21. Fagerholm SC, Varis M, Stefanidakis M, Hilden TJ, Gahmberg CG. alpha-Chain phosphorylation of the human leukocyte CD11b/CD18 (Mac-1) integrin is pivotal for integrin activation to bind ICAMs and leukocyte extravasation. *Blood*. 2006;108(10):3379–3386.
22. Lengyel E. Ovarian cancer development and metastasis. *Am J Pathol*. 2010;177(3):1053–1064.
23. Lu Z, Wang J, Wientjes MG, Au JL. Intraperitoneal therapy for peritoneal cancer. *Future Oncol*. 2010;6(10):1625–1641.
24. Abrahams VM, et al. Epithelial ovarian cancer cells secrete functional Fas ligand. *Cancer Res*. 2003;63(17):5573–5581.
25. Bjørge L, et al. Ascitic complement system in ovarian cancer. *Br J Cancer*. 2005;92(5):895–905.
26. Burleson KM, Casey RC, Skubitz KM, Pambuccian SE, Oegema TR, Skubitz AP. Ovarian carcinoma ascites spheroids adhere to extracellular matrix components and mesothelial cell monolayers. *Gynecol Oncol*. 2004;93(1):170–181.
27. Shield K, Riley C, Quinn MA, Rice GE, Ackland ML, Ahmed N. Alpha2beta1 integrin affects metastatic potential of ovarian carcinoma spheroids by supporting disaggregation and proteolysis. *J Carcinog*. 2007;6:11.
28. Condeelis J, Pollard JW. Macrophages: obligate partners for tumor cell migration, invasion, and metastasis. *Cell*. 2006;124(2):263–266.
29. De Palma M, Lewis CE. Macrophage regulation of tumor responses to anticancer therapies. *Cancer Cell*. 2013;23(3):277–286.
30. Qian BZ, Pollard JW. Macrophage diversity enhances tumor progression and metastasis. *Cell*. 2010;141(1):39–51.
31. Franklin RA, et al. The cellular and molecular origin of tumor-associated macrophages. *Science*. 2014;344(6186):921–925.
32. Chen J, et al. CCL18 from tumor-associated macrophages promotes breast cancer metastasis via PITPNM3. *Cancer Cell*. 2011;19(4):541–555.
33. Chen Q, Zhang XH, Massagué J. Macrophage binding to receptor VCAM-1 transmits survival signals in breast cancer cells that invade the lungs. *Cancer Cell*. 2011;20(4):538–549.
34. Qian BZ, et al. CCL2 recruits inflammatory monocytes to facilitate breast-tumour metastasis. *Nature*. 2011;475(7355):222–225.
35. Huang Y, Snuderl M, Jain RK. Polarization of tumor-associated macrophages: a novel strategy for vascular normalization and antitumor immunity. *Cancer Cell*. 2011;19(1):1–2.
36. Germano G, et al. Role of macrophage targeting in the antitumor activity of trabectedin. *Cancer Cell*. 2013;23(2):249–262.
37. Rolny C, et al. HRG inhibits tumor growth and metastasis by inducing macrophage polarization and vessel normalization through downregulation of PlGF. *Cancer Cell*. 2011;19(1):31–44.
38. McAllister SS, Weinberg RA. The tumour-induced systemic environment as a critical regulator of cancer progression and metastasis. *Nat Cell Biol*. 2014;16(8):717–727.
39. Kaplan RN, et al. VEGFR1-positive haematopoietic bone marrow progenitors initiate the pre-metastatic niche. *Nature*. 2005;438(7069):820–827.
40. Hanahan D, Weinberg RA. Hallmarks of cancer: the next generation. *Cell*. 2011;144(5):646–674.
41. Peinado H, Rafii S, Lyden D. Inflammation joins the "niche". *Cancer Cell*. 2008;14(5):347–349.
42. Robinson-Smith TM, et al. Macrophages mediate inflammation-enhanced metastasis of ovarian tumors in mice. *Cancer Res*. 2007;67(12):5708–5716.
43. Colegio OR, et al. Functional polarization of tumour-associated macrophages by tumour-derived lactic acid. *Nature*. 2014;513(7519):559–563.
44. Desgrosellier JS, Cheresh DA. Integrins in cancer: biological implications and therapeutic opportunities. *Nat Rev Cancer*. 2010;10(1):9–22.
45. Cui TX, et al. Myeloid-derived suppressor cells enhance stemness of cancer cells by inducing microRNA101 and suppressing the corepressor CtBP2. *Immunity*. 2013;39(3):611–621.
46. Pradeep S, et al. Hematogenous metastasis of ovarian cancer: rethinking mode of spread. *Cancer Cell*. 2014;26(1):77–91.
47. Reijnhart RM, Bieber MM, Teng NN. FACS analysis of peritoneal lymphocytes in ovarian cancer and control patients. *Immunobiology*. 1994;191(1):1–8.
48. Goswami S, et al. Macrophages promote the invasion of breast carcinoma cells via a colony-stimulating factor-1/epidermal growth factor paracrine loop. *Cancer Res*. 2005;65(12):5278–5283.
49. Russell S, Duquette M, Liu J, Drapkin R, Lawler J, Petrik J. Combined therapy with thrombospondin-1 type I repeats (3TSR) and chemotherapy induces regression and significantly improves survival in a preclinical model of advanced stage epithelial ovarian cancer. *FASEB J*. 2015;29(2):576–588.
50. Gordon IO, Freedman RS. Defective antitumor function of monocyte-derived macrophages from epithelial ovarian cancer patients. *Clin Cancer Res*. 2006;12(5):1515–1524.
51. English DP, et al. Solitomab, an epithelial cell adhesion molecule/CD3 bispecific antibody (BiTE), is highly active against primary chemotherapy-resistant ovarian cancer cell lines in vitro and fresh tumor cells ex vivo. *Cancer*. 2015;121(3):403–412.